

PRELIMINARIES TO MODELING AND ANALYSIS OF FUNCTIONALLY GRADED MATERIALS

Zahra Sharif Khodaei

Supervisor:
Ing. Jan Zeman, Ph.D.

Czech Technical University in Prague
Faculty of Civil Engineering
2005

TABLE OF CONTENTS

1	ABSTRACT	4
2	INTRODUCTION	4
2.1	PRODUCTION TECHNIQUES	5
2.1.1	<i>Routes based on conventional techniques</i>	5
2.1.2	<i>Non-conventional Methods</i>	8
2.2	ANALYSIS MODELS OF FGM MATERIALS	9
2.3	FEM/BEM COMPARISON	9
3	ANALYTICAL MODELING OF FMGS.....	10
3.1	MICROSTRUCTURAL MODEL	11
3.1.1	<i>Basic parameters</i>	11
3.1.2	<i>Statistical model</i>	12
3.1.3	<i>Examples</i>	14
3.2	SETTING OF THE MECHANICAL PROBLEM	18
3.3	NUMERICAL EXAMPLES	19
3.4	CONCLUSIONS.....	20
4	NUMERICAL MODELING OF FMGS USING HASHIN-SHTRIKMAN VARIATIONAL PRINCIPLES	20
4.1	CLASSICAL VARIATIONAL PRINCIPLES	20
4.2	HASHIN-SHTRIKMAN VARIATIONAL PRINCIPLES	21
4.2.1	<i>Comparison problem</i>	21
4.2.2	<i>Displacement field decomposition</i>	23
4.2.3	<i>Green's function method</i>	23
4.2.4	<i>Probabilistic averaging</i>	25
4.2.5	<i>Stationarity conditions</i>	27
5	FINITE ELEMENT METHOD	27
5.1	INTRODUCTION	27
5.2	SOLUTION $U^0(x)$	27
5.3	FUNCTION Γ^H	28
5.4	SOLUTION OF THE POLARIZATION PROBLEM	29
5.5	RESULTS POSTPROCESSING	31
5.6	ALGORITHMIC DETAILS OF FEM-HASHIN-SHTRIKMAN SOLUTION.....	31
6	BOUNDARY ELEMENT METHOD	32
6.1	BEM INTRODUCTION	32
6.2	BEM APPROXIMATION IN ONE DIMENSION.....	33

6.2.1	<i>Infinite body Green's function</i>	33
6.2.2	<i>General relations</i>	34
6.3	SOLUTION $U^0(x)$	36
6.4	SOLUTION $U^1(x; \alpha)$	36
6.5	POST-PROCESSING RESULTS	38
6.6	ALGORITHMIC DETAILS OF BEM-HASHIN-SHTRIKMAN SOLUTION	39
7	NUMERICAL EXAMPLES	39
7.1	FEM EXAMPLES	40
7.1.1	<i>Structure with non-uniform intensity</i>	40
7.1.2	<i>Example of structure with uniform intensity</i>	44
7.2	BEM EXAMPLES	45
8	CONCLUSIONS AND FUTURE WORK	47
9	REFERENCES	48
10	APPENDICES	49
10.1	SIMULATION METHOD	49
10.1.1	<i>Non-uniform intensity</i>	49
10.1.2	<i>Uniform intensity</i>	51
10.2	HASHIN-SHTRIKMAN FEM METHOD	53
10.3	HASHIN-SHTRIKMAN BEM METHOD	55

Nomenclature

ρ	Intensity
α	Number of realization
χ_m	Matrix characteristic function
χ_h	Reinforcement characteristic function
c_m	Local volume fraction of the matrix phase
c_h	Local volume fraction of the reinforce phase
$S_r(x)$	One point probability function
$S_{rs}(x,y)$	Two point probability function
L	Length of macrostructure
l	Length of microstructure
$EX(f(x))$	Expected value of a function f at a point x
E_m	Modulus of elasticity of the matrix phase
E_h	Modulus of elasticity of the reinforce phase
S	Set of all possible samples
$P(x, \alpha)$	Probability of α in s
$v(x)$	Test function
$\tau(x, \alpha)$	Polarization stress
$\Gamma_h(x, \alpha)$	Discretized value of strain Green's function
$\tau_r(x)$	Deterministic value of polarization stress for phase r
$N(x)$	Basis function
$B(x)$	Strain-displacement transformation matrix
r_u	Nodal displacement
r_τ	Value of polarization stress τ at integration points
K	Stiffness matrix
R	Vector of nodal loading
ξ	Integration points
h	Length of finite element
n	Number of finite elements
H	Heaviside step function
$\delta(x)$	Dirac delta function
δ_{rs}	Kronecker's delta

1 ABSTRACT

Functionally graded materials (FGMs) include a dual-phase graded layer in which two different constituents are mixed continuously and functionally according to a given volume fraction. For the analysis of their thermo-mechanical response, conventional overall (average, global or homogenized) methods have been widely employed in order to estimate equivalent material properties of the graded layer. However, such overall estimations are insufficient to accurately predict the local behavior.

In this project, a numerical procedure based on discretized Hashin-Shtrikman variational principles is introduced as an alternative to traditional approaches. After a brief review of state-of-the-art in the field of FMGs, we study a stochastic microstructural model for these materials in one dimension together with an appropriate boundary value problem to be solved. Next, the Hashin-Shtrikman variational principles are reviewed and applied to these material systems. The finite element and the boundary element method are used to discretize the resulting stationarity conditions. Finally, a number of numerical examples are presented to illustrate performance of these methods and show differences between the response of FGMs and composites with a uniform microstructure.

2 INTRODUCTION

Many components are subjected to mechanical, thermal or chemical loads that are unevenly distributed across their section. Gradient materials offer the possibility to combine two materials properties avoiding most of the disadvantages of a bimaterial. In contrast, traditional composites are homogeneous mixtures, and they therefore involve a compromise between the desirable properties of the component materials. Since significant proportions of an FGM contain the pure form of each component, the need for compromise is eliminated. The properties of both components can be fully utilized. For example, the toughness of a metal can be mated with the refractoriness of a ceramic, without any compromise in the toughness of the metal side or the refractoriness of the ceramic side. Consider for example a turbine blade which must withstand high non-stationary heat fluxes and centrifugal accelerations. An ideal structure for this application would consist of a tough metal core and a heat and corrosion resistant ceramic at the hot surface of the blade. If the ceramic is directly bonded to the metal, spalling may occur during thermal cycling as very high thermal stresses occur at the interface. A gradient material that has a smooth transition from the ceramic surface to the metal core can avoid the thermomechanical stress concentration at the interface.

The main feature of a gradient material is that its properties changes gradually with position. Used as coatings and interfacial zones, they help to reduce mechanically and thermally induced stresses caused by the material property mismatch and to improve the bonding strength.

From the beginning of introduction of FGMs (Functionally graded materials), conventional homogenization approaches such as the rules of mixtures, the mean-field micromechanics models, the unit cell model and so on for usual dual-phase composites have been employed. Even though these models provide reasonable overall prediction of thermo-mechanical behavior, these may fail to describe the reliable local behavior owing to the assumptions involved in them. In reality, the material properties of phase composites are function of shape and size, orientation and dispersion structure of constituent and the loading and the boundary conditions. Therefore, in order to predict the reliable local behavior of FGMs, one needs sort of discrete (or local) material property estimation techniques.

However, most of the “extreme environment” applications for FGMs require bulk FGMs, i.e., FGMs with gradient breadth in the order of millimeters to centimeters, and with continuous gradient profiles. Bulk FGMs remain merely a hypothesis. No commercially viable process has yet been developed to make such a material. While the scientific literature abounds in papers on the modeling of the hypothetical properties of bulk FGMs, the few proposed fabrication methods are labor-intensive specialized laboratory techniques, not low-cost commercial processes.

2.1 PRODUCTION TECHNIQUES

Due to intensive research efforts during the last ten years, a large spectrum of processing methods is available today. Only a few widespread methods that are applicable to a variety of material combinations shall be presented here.

Two classes of methods can be distinguished according to the way in which the gradient is created: In constructive processes the gradient is built up layer by layer from the constituents. A second class of routes relies on transport processes to build up the gradient. The transport processes may either soften the border between two phases or inversely a homogenous precursor material is graded in an external field, e.g. a temperature or electric field.

2.1.1 Routes based on conventional techniques

2.1.1.1 Powder metallurgy processing

FGM's can be produced by traditional powder processing routes if an additional step is introduced before consolidation. The gradation methods can be divided into dry and wet processes, where the powders are dispersed in a liquid medium.

Powder metallurgy offers more advantages by means of the lower costs, higher raw materials availability, simpler processing equipment, lower energy consumption and shorter processing

times. In a global sense the higher advantages in powder metallurgy, materials can be numbered as higher composition uniformity leading to segregation absence and a finer and more uniform distribution in the second phases as precipitates and carbides. It is especially important when the material is constituted by two or more bonded phases, matrix and reinforcement, trying to combine the most interesting properties of each one of them, in a composite material. Powder metallurgy offers the advantage, in front of other conventional techniques, of the possibility to obtain a composite material with higher content of reinforcement. Besides, another advantage of powder metallurgy is the possibility of changing the composition as a function of the requirements and with the aim of a FGM obtaining.

Dry processing. Powder compacts are usually prepared by stacking dry powders. The basic technique consists of appropriate composition and simply stacking one layer on top of the other. Dry stacking techniques will usually produce discrete layers with a minimum thickness of about 0.2 mm.

Multilayer techniques have serious constraints: they produce stepped gradients, and being batch processes, they are not suitable for mass production. Thus, there have been developed a continuous process, in which synchronized distributor places the different powders on a conveyor belt. Another process that produces stepless gradient is centrifugal powder metallurgy, where a powder of continuously varying composition is transferred onto a rotating plate, from where it is projected to the rotating wall of centrifuge. The process can be modified by mixing different amounts of filler materials instead of changing the powder composition. This enables production of porosity gradients.

Wet processing. Conventional powder processing is frequently modified by employing powder suspensions instead of the powders themselves. Aqueous suspensions of powders are sprayed from separate guns and drying takes place during the spraying process. This allows a very fine adjustment of the gradient as very thin layers may be stacked.

A widespread technique for ceramic/ceramic gradient material is sequential slip casting where slips of different composition are cast on top of the other. However, the production of metal-ceramic FGM's with this method is difficult, as very different powder particles sizes have to be used in order to adjust sintering rates. This leads to complications because high permeability differences inside the green body cause fracture during process. The key to successful fabrication of multiplayer metal-ceramic green bodies like in avoiding large differences in permeability and pore sizes between neighboring layers. Instead of slip casting, electrophoretic deposition from slurries of changing composition may be used to produce a graded green body.

It is also possible to produce smooth, stepless gradients by slip casting or pressure infiltration.

Transport processes like sedimentation or electrophoresis also allow production of continuously graded powder compacts. FGM's may also be produced from powders dispersed in the gas phase. For example, by continuously changing the precursor material in a mist pyrolysis process, a powder compact with a smooth gradient is retained after depositing the aerosol onto a filter.

Consolidation techniques. The main drawbacks of powder technology in FGM production, apart from processing costs, are the difficulties in consolidating the powder mixtures. One requirement for the successful consolidation of a dense graded powder compact is an equality between the initial packing density of the different powder mixtures, otherwise uneven shrinkage will lead to deformation of compact during sintering. A similarity of the sintering kinetics of the different composition is also required at all temperatures; otherwise the compact will warp and crack during sintering. For metal-ceramic FGM's the second requirement is usually not met and special techniques for the successful production of dense FGM's have to be developed.

2.1.1.2 Thermal Spray Techniques

Thermal spray techniques are very attractive methods of production of FGM coatings as they are suitable for metals and refractory materials. Thermal spray is a generic term for a group of coating processes used to apply metallic or nonmetallic coatings. These processes are grouped into three major categories: flame spray, electric arc spray, and plasma arc spray. These energy sources are used to heat the coating material (in powder, wire, or rod form) to a molten or semimolten state. The resultant heated particles are accelerated and propelled toward a prepared surface by either process gases or atomization jets. Upon impact, a bond forms with the surface, with subsequent particles causing thickness buildup and forming a lamellar structure.

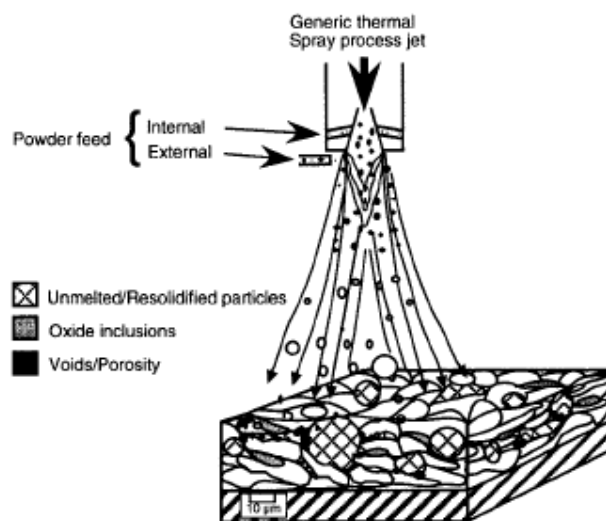


Figure 1 Thermal spray process

2.1.1.3 Coating Techniques

A number of existing coating techniques can be modified in such a way that a gradation is introduced by changing the composition of the precursor material. The most important class of deposition processes uses vaporized precursor materials. These vapor deposition techniques allow for production of thin coatings only, typically in the range of micrometer. The gradient is produced by proper amount of precursors of a reactive gas such as oxygen or nitrogen in the deposition chamber. However, the relationship between composition of the gas phase and the produced films is not always simple. The design of gradients by these processes may thus be a tedious procedure and requires investigation of film growth and composition for different gas phase compositions.

2.1.1.4 Other methods

Thin-sheet lamination is a very attractive method to produce step-like gradient, because of its low cost and suitability for mass production. Step-graded ceramic coating can also be produced by repeatedly dipping a substrate into slurries of varying composition and drying. Stacking of 2D-fabrics with powder coating of different thickness or composition and subsequent hot pressing will result in a functionally graded fiber composites.

Diffusion bonding is a simple and cost effective gradation method for the case that the gradation profile is not very important and only a thin graded layer is required.

2.1.2 Non-conventional Methods

There is a number of manufacturing routes for FGM's that are not directly derived from conventional techniques. In general these methods are not as good as the conventional methods, but some of them deserve attention as they have particular advantages, like low-cost or the possibility to produce particular microstructures.

One of these methods is infiltration techniques, which are suitable methods for material combination with very different melting points.

For the production of purely metallic FGM's, thermomechanical processes can be used. Recently, much interest has been raised in developing new processing techniques, which can be used to produce continuously graded composition. Centrifugal casting, continuous casting, infiltration, co-sedimentation, etc. are newly developed methods. Of these methods, co-sedimentation is special due to its simple operation, low consumption, and the characteristics suitable for most FGM systems.

To conclude, there are a lot of production methods for FGM's, each having its advantages. Which of these methods is suitable depends on the material system, the kind of gradation needed

and the required microstructure and density of the product.

2.2 ANALYSIS MODELS OF FGM MATERIALS

The main advantage of a gradient in a material is that it offers the possibility to optimize a particular property of a material while maintaining other properties within acceptable limits. In order to maximize the use of the FGM concept it is necessary to determine the optimum composition profile by appropriate modeling studies as the large number of possible gradation renders an experimental study impracticable.

The estimation of material properties for phase composites can be classified into theoretical and experimental categories. The theoretical approaches are split into microscopic and overall studies. The prediction methods of overall material properties are generally classified into three groups: (a) direct, (b) variational and (c) approximation approaches. The direct method seeks closed-form analytic solution; therefore a precise mathematical treatment becomes troublesome. On the other hand, the variational method such as Hashin Shtrikman's bounds does not specify the details in the phase geometry but rather provide the upper and lower bounds for the overall properties.

In the approximation approach, the self-consistent model by Hill and the others, the mean field micro-mechanics models by Mori and Tanaka and Wakashima and Tsukamoto, The linear and modified rules of mixtures by Tamura and the unit cell model by Ravichandran are widely-employed overall estimates [11]. These overall models are simple and convenient to predict the overall thermo-mechanical response and material properties.

2.3 FEM/BEM Comparison

1. **FEM:** An entire domain mesh is required.

BEM: A mesh of the boundary only is required.

Comment: Because of the reduction in size of the mesh, one often hears of people saying that the problem size has been reduced by one dimension. This is one of the major pluses of the BEM - construction of meshes for complicated objects, particularly in 3D, is a very time consuming exercise.

2. **FEM:** Entire domain solution is calculated as part of the solution.

BEM: Solution on the boundary is calculated first, and then the solutions at domain points (if required) are found as a separate step.

Comment: There are many problems where the details of interest occur on the boundary, or are localized to a particular part of the domain, and hence an entire domain solution is not required.

3. **FEM:** Differential Equation is being approximated.

BEM: Only boundary conditions are being approximated.

Comment: The use of the Green-Gauss theorem and a fundamental solution in the formulation means that the BEM involves no approximations of the differential Equation in the domain - only in its approximations of the boundary conditions.

4. **FEM:** Sparse symmetric matrix generated.

BEM: Fully populated non-symmetric matrices generated.

Comment: The matrices are generally of different sizes due to the differences in size of the domain mesh compared to the surface mesh. There are problems where either method can give rise to the smaller system and quickest solution - it depends partly on the volume to surface ratio. For problems involving infinite or semi-infinite domains, BEM is to be favoured.

5. **FEM:** Element integrals easy to evaluate.

BEM: Integrals are more difficult to evaluate, and some contain integrands that become singular.

Comment: BEM integrals are far harder to evaluate. Also the integrals that are the most difficult (those containing singular integrands) have a significant effect on the accuracy of the solution, so these integrals need to be evaluated accurately.

6. **FEM:** Widely applicable. Handles nonlinear problems well.

BEM: Cannot even handle all linear problems.

Comment: A fundamental solution must be found (or at least an approximate one) before the BEM can be applied. There are many linear problems (e.g., virtually any non-homogeneous equation) for which fundamental solutions are not known. There are certain areas in which the BEM is clearly superior, but it can be rather restrictive in its applicability.

7. **FEM:** Relatively easy to implement.

BEM: Much more difficult to implement.

Comment: The need to evaluate integrals involving singular integrands makes the BEM at least an order of magnitude more difficult to implement than a corresponding finite element procedure.

In this paper we will study the modeling of FGM material first by Monte-Carlo simulation method and compare the result with Hashin Shtrikman's variational method. This text is followed by a computer program which studies the material properties achieved by these two methods. For full review of the programs, see appendices.

3 Analytical modeling of FMGs

In the field of material science, there have been many studies of functionally graded materials. Recall that FMGs are made of continuously gradient heterogeneous materials, and offer desired functions which are adaptive to the environmental situations. In the conventional modeling of FMGs, the rule of mixture has been most frequently used.

Real world functionally graded materials, such as biological cellular materials, however, exhibit very complex microstructures. Therefore they may exhibit many interesting and important macroscopic functions such as foam materials with negative Poisson's ratio, or human bone, possessing layered microstructure architecture. Obviously, the macroscopic properties of these cellular materials cannot be accurately described by the rule of mixtures. Hence, a more general model is needed.

The model introduced in the current work systematically builds on a realistic description of graded composite geometry, see Section 3.1. Due to the random nature of the problem, the adopted description is based on the theory of non-uniform Poisson processes. After the statistical characterization of the model, the mechanical problem to be solved is introduced in Section 3.2. Finally, the analytical expression for mean values of selected quantities of interest is presented in Section 3.3 to provide a basis for assessment of performance of numerical approximation methods in Chapters 4–7 where the structure is solved by FEM and BEM and a comparison is being made.

3.1 Microstructural model

3.1.1 Basic parameters

The microstructural model adopted in this work is basically a one-dimensional variant of the geometrical model proposed by Quintanilla and Torquato [1]. The schematic illustration of the model is shown in Figure 2. The macroscopic structure is understood as a rod of length L with reinforcements of length l distributed within the structure. It is tacitly assumed that $l \ll L$, so that a direct simulation (especially for more dimensional cases) would be practically intractable. The position of individual reinforcements follows from coordinates of *reference points* x_1, x_2, \dots, x_N randomly generated in the interval $\langle 0; L \rangle$.

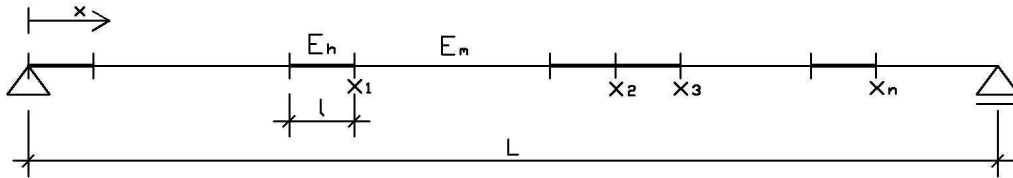


Figure 2 Scheme of the structure

To allow for microstructure gradation, the distribution of the reference points is specified using *position-dependent intensity* $\rho(x)$ giving the expected number of reference points $dn(x)$ found in an infinitesimal segment dx around a point x

$$dn(x) = \rho(x) dx \quad (3.1)$$

Therefore, the expected number of reference points found in a finite-size interval $I \subseteq \langle 0, L \rangle$ is

determined by

$$n(I) = \int_I \rho(x) dx. \quad (3.2)$$

Eq. (3.2) readily provides the number of reference points in the whole structure N

$$N = \left\lfloor n(\langle 0, L \rangle) \right\rfloor = \left\lfloor \int_0^L \rho(x) dx \right\rfloor, \quad (3.3)$$

where $\lfloor n \rfloor$ denotes the integer part of a variable n . Note that for a *statistically uniform* composites, the intensity $\rho(x) = \rho = \text{const}$ and Eq.(3.2) reduces to

$$n(I) = \rho |I|, \quad (3.4)$$

where $|I|$ denotes the length of an interval I .

3.1.2 Statistical model

3.1.2.1 Basic relations

To provide a general framework for the description of the introduced microstructural model, we firstly introduce a concept of a *sample space* S (often denoted as an ensemble in statistical physics literature), denoting in our context the set of all possible microstructural configurations. Further, we label individual samples as $\alpha \in S$. Then, the *expected value* (or ensemble average) $EX(f(x))$ of a random function $f(x; \alpha)$ is defined as

$$EX(f(x)) = \int_S f(x, \alpha) p(\alpha) d\alpha, \quad (3.5)$$

where $p(\alpha)$ denotes the probability density of α in S .

Note that when a direct simulation method is used to estimate the expected value $EX(f(x))$, $\alpha \in \{1, 2, 3, \dots, |S|\}$ (with $|S|$ denoting the number of samples), each sample α has equal probability $p(\alpha) = 1/|S|$ and the expected value is provided by

$$EX(f(x)) = \frac{1}{|S|} \sum_{\alpha=1}^{|S|} f(x, \alpha). \quad (3.6)$$

Since the proposed model incorporates only binary (two-phase) heterogeneous materials, specification of the material distribution can be formally provided by the *matrix characteristic function* χ_m :

$$\chi_m(x, \alpha) = 1 \Leftrightarrow x \text{ is in the matrix phase for the sample } \alpha. \quad (3.7)$$

Complementary, we can define the *heterogeneity characteristic function* χ_h as

$$\chi_h(x, \alpha) = 1 \Leftrightarrow x \text{ is in the reinforcing phase for the sample } \alpha. \quad (3.8)$$

Clearly, characteristic functions for individual phases are not independent as

$$\chi_m(x, \alpha) + \chi_h(x, \alpha) = 1. \quad (3.9)$$

3.1.2.2 Local volume fractions

The basic statistical description of the considered material system is provided by the expected value of the matrix characteristic function. It follows from relations (3.7) and (3.9) that the expected value coincides with the probability, that a point x will be located in the matrix phase; in other words with the probability that the interval $I(x)$, defined as

$$I(x) = \langle 0, L \rangle \cap \langle x-l, x \rangle \quad (3.10)$$

will not be occupied by any reference point. Recognizing that the distribution of individual reference points can be mathematically described as a non-uniform Poisson process, this probability can be determined as [2]

$$c_m(x) = \exp\left(-\int_{I(x)} \rho(t) dt\right). \quad (3.11)$$

In the following text, we will denote this quantity as a *local volume fraction* of the matrix phase and denote it as $c_m(x)$. It should be emphasized, however, that this term was selected only for notational convenience; it has nothing to do with volume average of the matrix characteristic function as in the case of unbounded statistically homogeneous composites [9]. Finally, it directly follows from Eq. (3.9) that the local volume fraction function for the reinforcement phase $c_h(x)$ is given by the relation

$$c_h(x) = \text{EX}(\chi_m(x)) = 1 - c_m(x). \quad (3.12)$$

3.1.2.3 Two-point probability functions

The previously introduced concept of a local volume fraction can be immediately used for simple averaging-based procedures such as rules of mixture. Nevertheless, when using more sophisticated approaches, more information on the microstructure is needed. Such a data can be provided by two-point probability functions, which give the probability, that given points x and y will be occupied by a prescribed phase. For example, the matrix-matrix probability function is follows from

$$S_{mm}(x, y) = \text{EX}(\chi_m(x) \chi_m(y)). \quad (3.13)$$

Using similar reasoning as for the case of local volume fractions, this relation coincides with the probability, that interval $I_2(x, y)$ given by

$$I_2(x, y) = I(x) \cup I(y) \quad (3.14)$$

will not be occupied by any reference point. Hence, the matrix-matrix probability function follows from

$$S_{mm}(x, y) = \exp\left(-\int_{I(x) \cup I(y)} \rho(t) dt\right). \quad (3.15)$$

Note due to relation (3.9), we can simply determine the remaining two-point probability functions (S_{mh} , S_{hm} , S_{hh}) once the S_{mm} is known:

$$\begin{aligned} S_{hm}(x, y) &= c_m(y) - S_{mm}(x, y), \\ S_{mh}(x, y) &= c_m(x) - S_{mm}(x, y), \\ S_{hh}(x, y) &= 1 - c_m(y) - c_m(x) + S_{mm}(x, y). \end{aligned}$$

3.1.3 Examples

To illustrate the theoretical results derived in this section, we select a simple model of a functionally graded material with a piecewise-linear distribution of intensity ρ . The particular form is motivated by a example of microstructure shown in Figure 3.

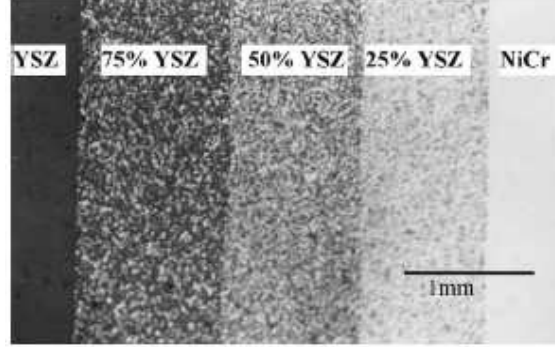


Figure 3 Example of a functionally graded material [3]

In this case, the parameterization of intensity profile is given by relations

$$\rho(x) = \begin{cases} \rho_a & 0 \leq x < a, \\ \rho_a + k_\rho(x-a) & a \leq x < b, \\ \rho_b & b \leq x \leq L. \end{cases} \quad (3.16)$$

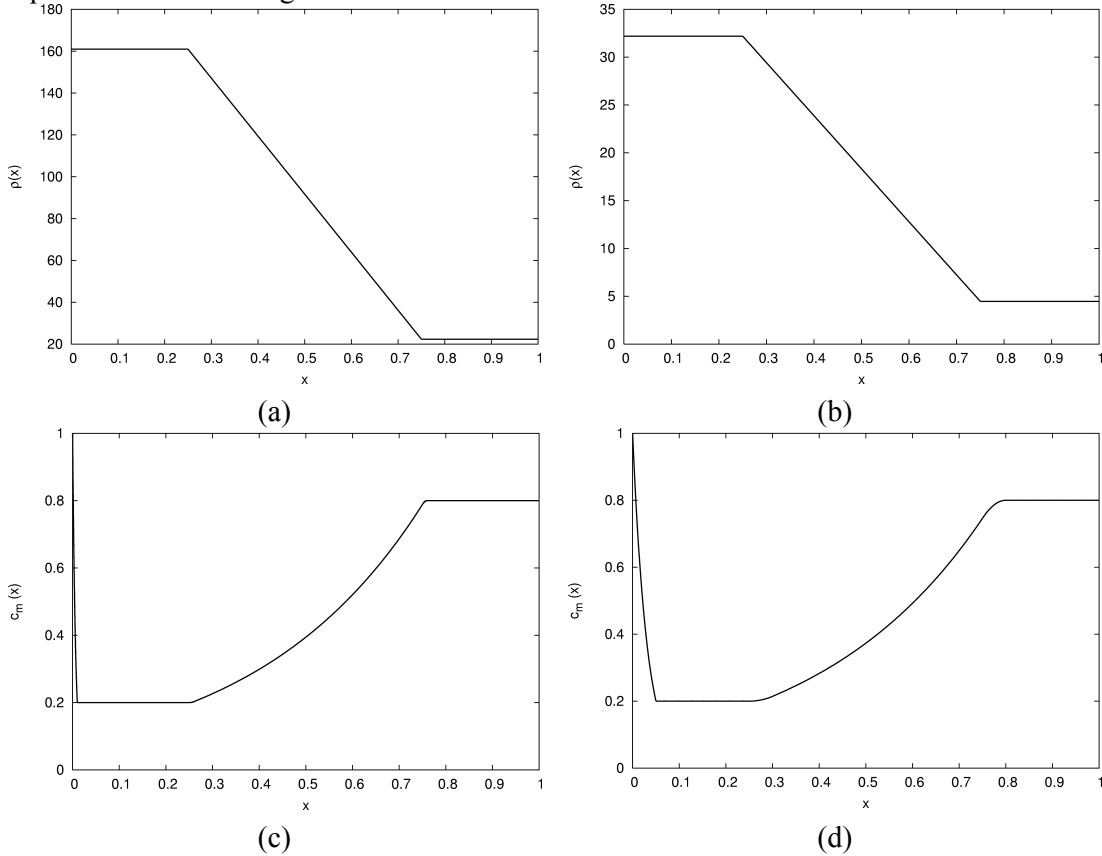
This form was selected mainly for the analytical convenience, considering e.g. piecewise constant distribution is clearly possible in this setting without any problems. Furthermore, by selecting $\rho_a = \rho_b$ we immediately recover the case of statistically homogeneous composite. The first geometrical quantity is the expected number of reference points in the whole structure. It directly follows from relation (3.3):

$$N = \left\lfloor \frac{1}{2} \left((a+b)\rho_a + (2L-a-b)\rho_b \right) \right\rfloor. \quad (3.17)$$

The expression for the local matrix volume fraction is a little bit more involved; after some elementary, but rather tedious, manipulation we obtain

$$c_m(x) = \begin{cases} \exp(-\rho_a x) & 0 \leq x \leq l, \\ \exp(-\rho_a l) & l < x \leq a, \\ \exp\left(-\rho_a l - \frac{k_\rho}{2}(x-a)^2\right) & a < x \leq a+l, \\ \exp\left(-\rho_a l - \frac{k_\rho}{2}l(2(x-a)-l)\right) & a+l < x \leq b, \\ \exp\left(-\rho_b l + \frac{k_\rho}{2}(x-b-l)^2\right) & b < x \leq b+l, \\ \exp(-\rho_b l) & b+l < x \leq L. \end{cases} \quad (3.18)$$

The character of the local volume fraction is illustrated on Figure 3(a)—(f). Geometrical parameters of the model are set to $L=1\text{m}$, $a=0.25\text{m}$ and $b=0.25\text{m}$. The selected profiles of intensity are shown in Figure 3 (a) for $l=0.01\text{m}$ and for $l=0.05\text{m}$ in Figure 3(b). In both cases, the quantities ρ_a and ρ_b were selected in such a way, that local volume fractions equal to 20% and 80% in the non-graded parts of the structure. The resulting local volume fractions are shown in Figure 3(c)—(d), while Figure 3(e)—(f) show corresponding profiles for statistically homogeneous composites with intensity defined in such a way that number of reference points is equal to the non-homogeneous case.



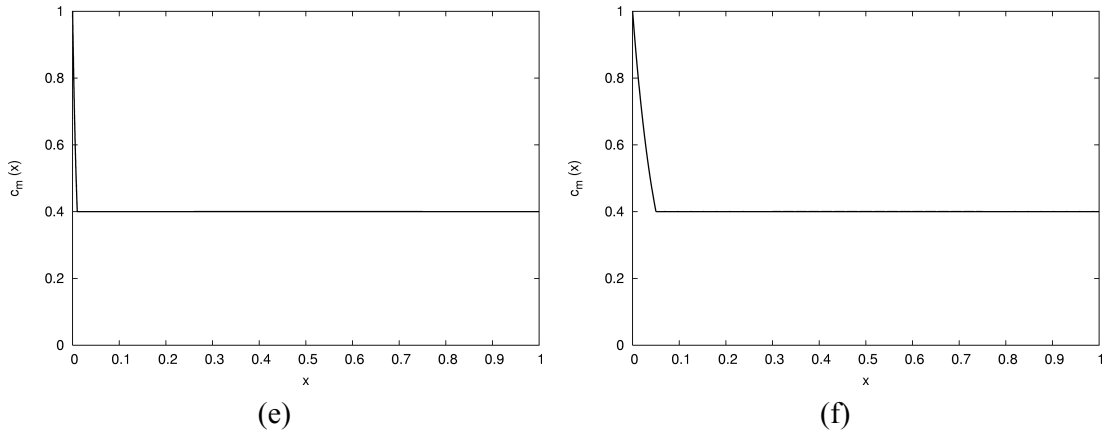
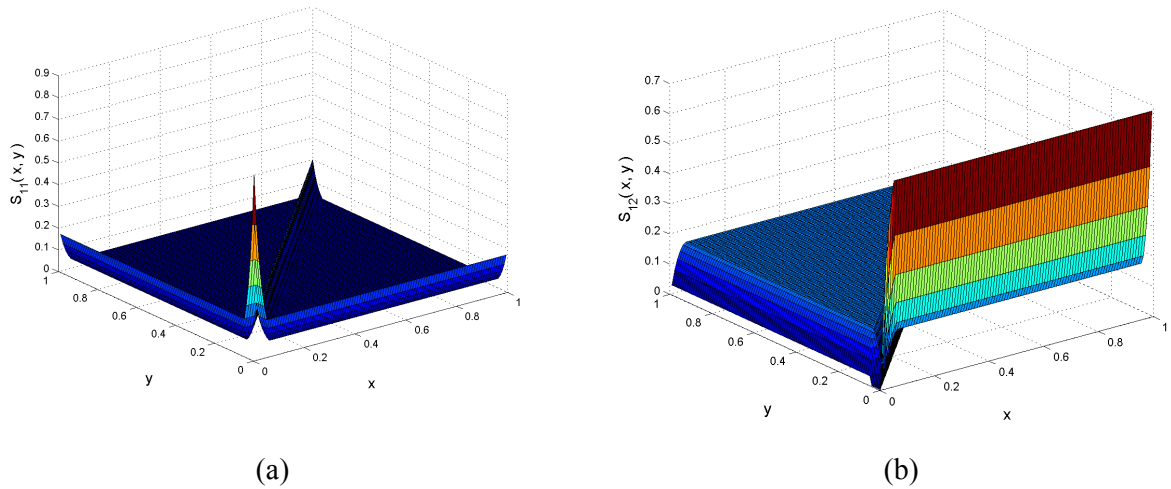
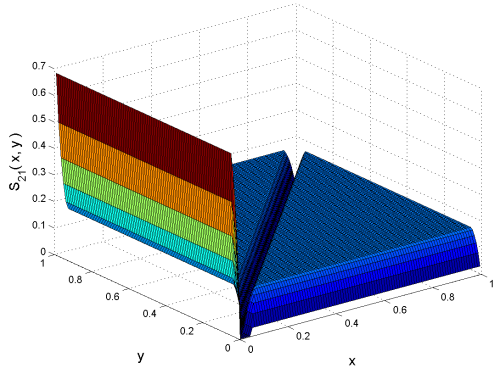


Figure 4 (a,b) Profiles of intensity for $l=0.01$ and $0.05m$, (c,d) Local volume fractions for a statistically *non-uniform* composite, (e,f) Local volume fractions for a statistically *uniform* composite

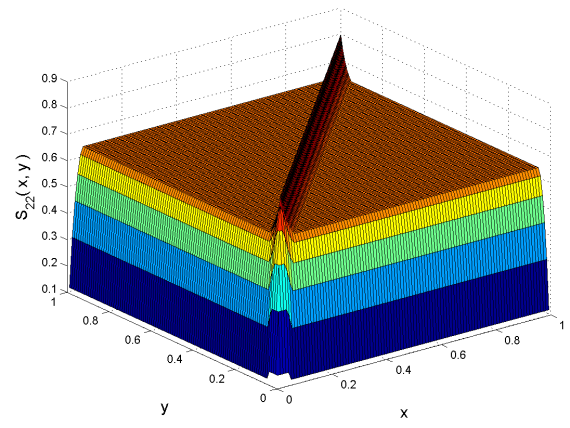
The resulting dependencies nicely illustrate the basic features of functionally-graded materials which are not present in traditional homogenization of statistically homogeneous composites. First, the *size effects* demonstrated by different profiles of local volume fraction for different sizes of reinforcements; compare Figure 3(c,e) with Figure 3(d,f). Second, the *boundary layer* in the interval $(0,l)$. Although this phenomenon is present for both statistically uniform and non-uniform case, in a traditional analysis of composite materials it is usually neglected. For the functionally graded materials, however, this effect should be taken into account as it is comparable to microstructure gradation inside the heterogeneous body.

The two-point probability functions for a given microstructural model are summarized in Figure 5. Clearly, it contains substantially more information when compared to the two-point probability function. Note again the typical boundary layer present in the current microstructural model.

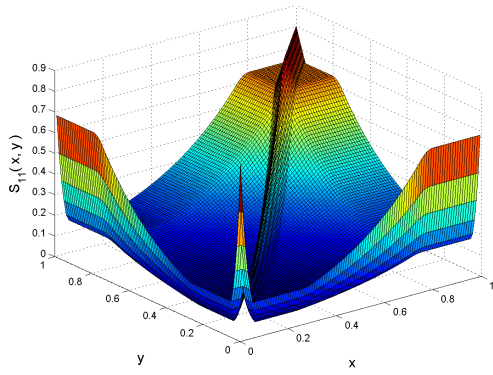




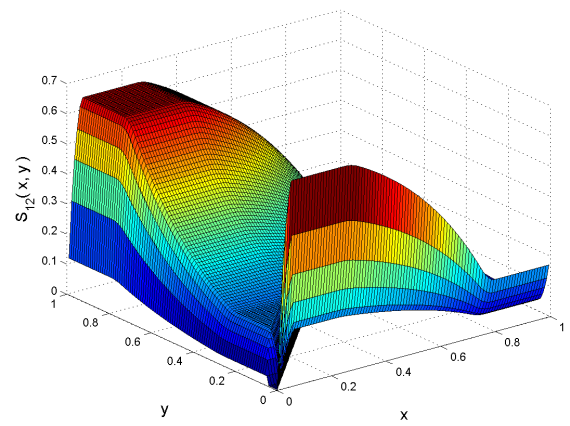
(c)



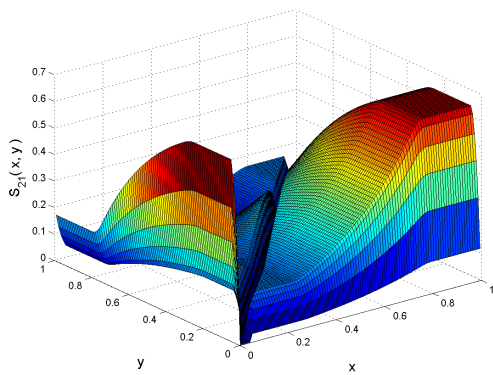
(d)



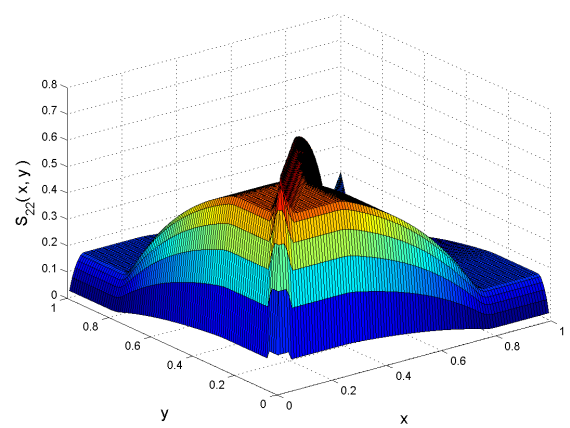
(e)



(f)



(g)



(h)

Figure 5 Examples of two-point probability functions, (a)—(d) statistically uniform composite, (e)—(h) statistically non-uniform composite

3.2 Setting of the mechanical problem

The particular structure studied in this section is shown in Figure 6.

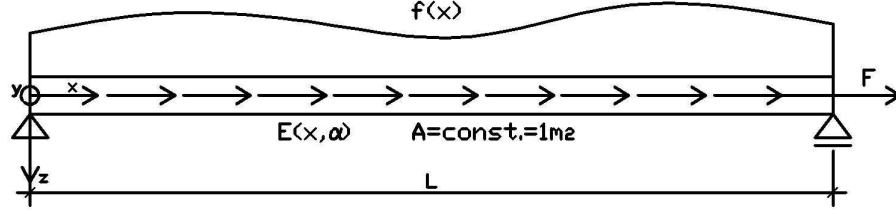


Figure 6 Setting of the mechanical problem

The *stochastic* boundary value problem (BVP) to be solved has the following form

$$-\frac{d}{dx} \left(E(x; \alpha) \frac{du(x; \alpha)}{dx} \right) = f(x) \quad (3.19)$$

with boundary conditions

$$\begin{aligned} u(0) &= 0, \\ E(L; \alpha) \frac{du(L; \alpha)}{dx} &= F, \end{aligned}$$

where α denotes the given realization of microstructure and remaining symbols follow from Figure 6. To keep the presentation simple, we concentrate on the determination of expected value of the displacement at a point x

$$\text{EX}(u(x)) = \int_s u(x; \alpha) p(\alpha) d\alpha, \quad (3.20)$$

where $u(x; \alpha)$ is a solution to the problem (3.19). Due to one-dimensional nature of the problem, we are able to determine this value analytically. In particular, we know that the normal force N is a deterministic value due to one-dimensional equilibrium conditions. Hence, for a given realization α , the displacement field u can be easily obtained as

$$u(x; \alpha) = \int_0^x \frac{N(t)}{E(t; \alpha)} dt. \quad (3.21)$$

Inserting Eq. (3.21) into averaging relation (3.20), we immediately see that

$$\text{EX}(u(x)) = \int_0^x N(t) \text{EX} \left(\frac{1}{E(t)} \right) dt, \quad (3.22)$$

where the expected value is provided by

$$\text{EX} \left(\frac{1}{E(t)} \right) = \frac{c_m(t)}{E_m} + \frac{c_h(t)}{E_h} = \frac{1}{E_h} + c_m(t) \left(\frac{1}{E_m} - \frac{1}{E_h} \right) \quad (3.23)$$

with local volume fractions given by Eqs. (3.11) and (3.12).. Observe that, as typical for one-dimensional statically determinate, the actual result depends only on the local volume fractions. This is rather an exception, considering a slightly more complex problem (e.g. statically indeterminate) would lead to more complex dependencies.

3.3 Numerical examples

To verify the introduced formulas and to illustrate problems encountered when dealing with random composites, we compute response of the material using a simple Monte-Carlo simulation technique. To this end, the microstructure is randomly generated using the algorithm described in Section 10.1, see also [1] for more details. Then, for every realization α , the displacement $u(x; \alpha)$ is determined by a direct integrations, see Eq. (3.21). Averaging these distributions according to Eq. (3.6) yields, as the number of samples goes to infinity, the theoretical value (3.22). In the following, we illustrate two results – one related to a variable $\rho(x)$ and one to a constant value. Further details about the algorithm used can be found in Section 10.1.

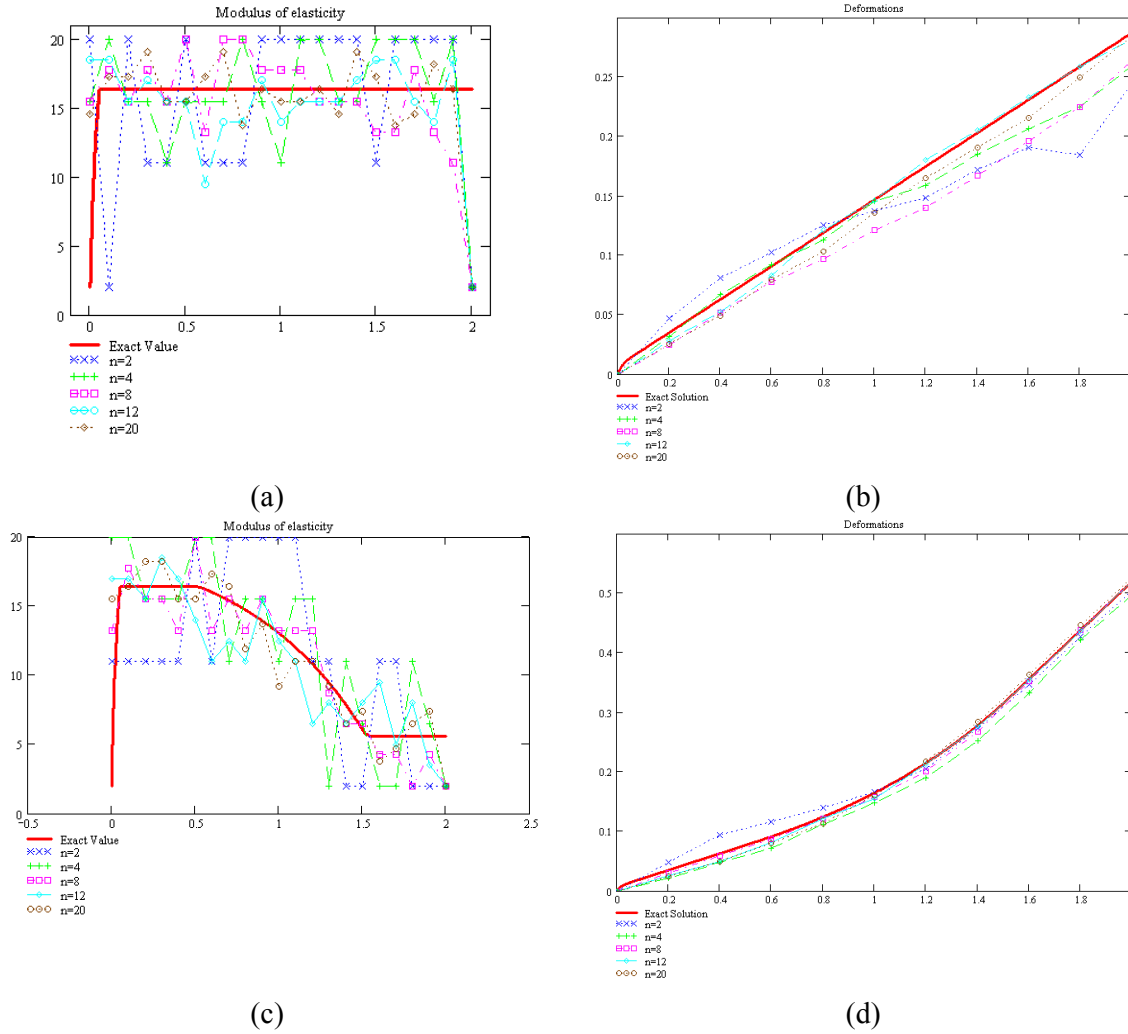


Figure 7 Direct simulation method, (a) Expected value of modulus of elasticity $EX(E(x))$ for a statistically homogeneous material, (b) Expected value $EX(u(x))$ for $F=0N, f=1 \text{ Nm}^{-1}$, (c) Expected value of modulus of elasticity $EX(E(x))$ for a statistically non-homogeneous material, (b) Expected value $EX(u(x))$ for $F=0N, f=1 \text{ Nm}^{-1}$. In all examples $E_m = 2\text{Pa}$, $E_h = 20 \text{ Pa}$, $L=2\text{m}$, $l=0.05\text{m}$,

3.4 Conclusions

As it is seen from the graphs in Figure 7, the analytical solution is converging to the theoretical solution (Exact solution). According to the results for $u(x)$, it is seen that a large number of realizations is not necessary to get a good result, although it takes time for the program to calculate the results. So it could be concluded that the Monte-Carlo approximation can be used and it gives a good approximation but it is time consuming, which is not very convenient. This is particularly visible for the approximation of $EX(E(x))$, which is rather poor even for a large number of realizations. The quality of numerical data is especially bad in the region of the boundary layer, which is perhaps of the most interest from the applications point of view.

This problem can be circumvented using proper numerical methods (FEM, BEM), since there is no need for number of realizations. Both of these methods are for the discretization of the Hashin-Shtrikman variational principles, which as summarized below.

4 Numerical modeling of FMGs using Hashin-Shtrikman variational principles

In their recent works, Luciano and Willis [2] and Procházka a Šejnoha [10] developed an approach, based on a stochastic variational principle. It generated an integral equation, whose kernel was related to a Green's function defined for the body in question. Such a Green's function can only be found explicitly for simple geometries, hence a proper numerical treatment is needed. The formulation leads directly to equations that provide representations for the stress and strain fields in any realization of the medium, from which any statistical average or local quantities can be computed. Explicit approximation is performed within a realization of Hashin-Shtrikman type for the stochastic variational structure.

In this Section, we basically follow the route set by Luciano and Willis, but we for a moment do not stick to any particular numerical method but rather provide a general framework for analysis composites on bounded domain. To allow the analysis for different geometries, the unknowns in Hashin-Shtrikman VP can be computed from FEM or BEM, which both of them are explained in more detail in Chapters 5 and 6.

4.1 Classical variational principles

First we recall the classical variational principles (VPs). Assume a simply supported beam with distributed normal loading $f(x)$ and applied force F at the end of the beam with variable and random modulus of elasticity $E(x;\alpha)$ as in Figure 5.

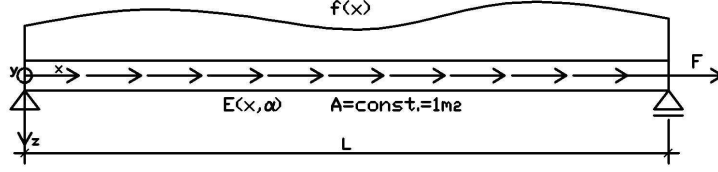


Figure 8 Example

The classical Lagrange variational principle suggest that from all the kinematically admissible states of the examined elastic body, the right is the one which gives the minimum value to the total potential (or complementary) energy:

$$\Pi = W + L \rightarrow \min \quad (3.24)$$

where W is internal energy, while L is the external energy (potential energy of external forces).

For this example we get:

$$\Pi(v; \alpha) = \int_0^L \left\{ \frac{1}{2} E(x; \alpha) \varepsilon(v(x))^2 - f(x)v(x) \right\} dx - Fv(L) \quad (3.25)$$

The minimization of $\Pi(v, \alpha)$ is performed on trial function which satisfy $v(0) = 0$. The minimizer $u(x; \alpha)$ of (3.25) satisfies the Euler equation

$$\delta \Pi(u(x; \alpha); \alpha) = \int_0^L \{ \varepsilon(\delta v(x)) E(x; \alpha) \varepsilon(u(x; \alpha)) - f(x) \delta v(x) \} dx = 0, \quad (3.26)$$

which must hold for all test functions δv verifying $\delta v(0) = 0$. This yields to the already introduced stochastic ODE, see (3.19),

$$\frac{d}{dx} (E(x; \alpha) \varepsilon(x; \alpha)) + f(x; \alpha) = 0. \quad (3.27)$$

Owing to the fact we study the problem with random coefficients, we introduce the stochastic variational principle:

$$\min_s EX(\Pi(v)) = \min \int_s \Pi(v; \alpha) p(\alpha) d\alpha \quad (3.28)$$

The minimizer of this expression provides the sought function $EX(u(x))$ presenting the solution to the problem.

4.2 Hashin-Shtrikman variational principles

4.2.1 Comparison problem

Following the original Hashin and Shtrikman idea, we consider two equivalent problems. First, the “real body”, which is a rod subjected to a uniform loading $f(x)$ and an applied concentrated force F at the end of the beam. The beam is from a heterogeneous random material, therefore the modulus of elasticity is denoted as $E(x; \alpha)$. The “comparison body” is introduced in Figure 7, which is identical in geometry and loading to the real body in Figure 6, with the difference that the modulus of elasticity, E_0 is assumed to be constant through the whole beam. To get an equivalent problem, the polarization stress τ is added to account for the difference between these two bodies. The aim here is to get the displacement u using the “comparison problem”. To this

end, we employ the Hashin-Shtrikman VP, where the unknowns are the polarization stress τ and the displacement field u .

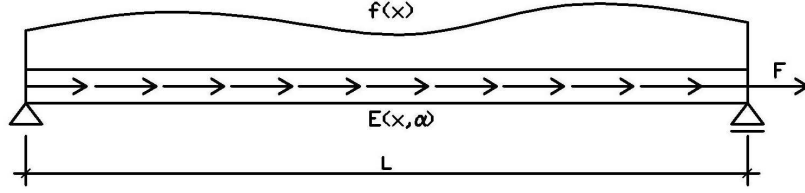


Figure 9 Real body

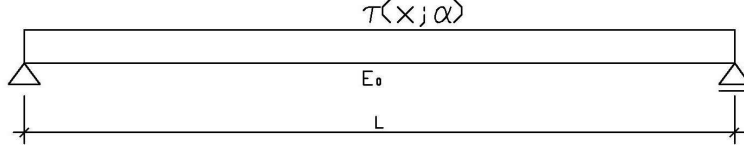


Figure 10 Comparison body

$$\begin{array}{ll} \text{Real body:} & \text{Comparison body:} \\ \sigma(x; \alpha) = E(x; \alpha)\varepsilon(x; \alpha) & \sigma(x; \alpha) = E_0\varepsilon(x; \alpha) + \tau(x; \alpha) \end{array} \quad (3.29)$$

In particular, the Hashin-Shtrikman functional for the current problem has the following form.

$$\begin{aligned} U(v, \tau, \alpha) = & \int_0^L \left\{ \frac{1}{2} E_0 \varepsilon(v(x))^2 + \tau(x; \alpha) \varepsilon(v(x)) - f(x)v(x) \right\} dx - Fv(L) \\ & + \int_0^L \frac{1}{2} [E(x; \alpha) - E_0]^{-1} \tau^2(x) dx \end{aligned} \quad (3.30)$$

It can be shown the saddle point of the functional delivers the value of displacement field $u(x, \alpha)$ and the true polarization stress $\tau(x, \alpha)$. Here v is a test function, τ is trial polarization stress and α denotes a realization. To demonstrate the equivalence between the Hashin-Shtrikman functional (3.30) and the original formulation, we need to subject $U(v; \tau, \alpha)$ to variation once with respect to τ and once with respect to v . The variation with respect to polarization stress leads to

$$\delta_\tau U(v, \tau, \alpha) = \int_0^L \delta\tau(x) \varepsilon(v(x)) + \delta\tau(x) [E(x; \alpha) - E_0]^{-1} \tau(x) dx = 0$$

for all variations $\delta\tau$. Hence,

$$\varepsilon(v(x)) + [E(x; \alpha) - E_0]^{-1} \tau(x) = 0 \Rightarrow E(x; \alpha)\varepsilon(x; \alpha) = E_0\varepsilon(x; \alpha) + \tau(x)$$

which corresponds to the stress equivalence condition (3.29). The stationarity condition with respect to v gives the condition:

$$\delta_u U(v, \tau, \alpha) = \int_0^L \varepsilon(\delta v(x)) E_0 \varepsilon(v(x)) + \tau(x; \alpha) \varepsilon(\delta v(x)) - f(x) \delta v(x) dx$$

Once we have established the validity of stress equivalence condition, the previous equation is clearly equivalent to the statement (3.26). Hence, these two problems are equivalent.

4.2.2 Displacement field decomposition

From the point of view of numerical treatment of the problem, we introduce the following split of displacement field

$$u(x; \alpha) = u^0(x) + u^1(x; \alpha) \quad (3.31)$$

where $u^0(x)$ is the displacement of the comparison body from loading which is known, and $u^1(x; \alpha)$ is the displacement from the polarization stress which is our additional unknown. First we write the stationarity conditions with respect to v . Similarly to (3.31), the test function $v(x)$ can be divided into:

$$v(x) = v^0(x) + v^1(x) \quad (3.32)$$

With this split, the Hashin-Shtrikman functional has the following form

$$\begin{aligned} U(v, \tau, \alpha) = & \int_0^L \frac{1}{2} [\varepsilon(v^0(x)) + \varepsilon(v^1(x))] E_0 [\varepsilon(v^0(x)) + \varepsilon(v^1(x))] \\ & + \tau(x; \alpha) [\varepsilon(v^0(x)) + \varepsilon(v^1(x))] - f(x)v^0(x) + \varepsilon(v^1(x))dx \\ & - F(v^0(L) + v^1(L)) - \frac{1}{2} \int_0^L \tau(x; \alpha) (E(x; \alpha) - E_0)^{-1} \tau(x; \alpha) dx \end{aligned} \quad (3.33)$$

Recall that $u^0(x)$ is a solution for a problem with known deterministic loading without the polarization stress. Hence it satisfies the condition:

$$\int_0^L [\varepsilon(\delta v^1(x)) E_0 \varepsilon(u^0(x; \alpha)) - \delta v^1(x) f(x)] dx - \delta v^1(L) F = 0 \quad (3.34)$$

Similarly, $u^1(x; \alpha)$ follows from variational equation

$$\int_0^L [\varepsilon(\delta v^0(x)) E_0 \varepsilon(u^1(x; \alpha)) + \delta \varepsilon(v^0(x)) \tau(x; \alpha)] dx = 0 \quad (3.35)$$

Therefore, at the saddle point, the value of the Hashin-Shtrikman functional equals to

$$\begin{aligned} U(u(x; \alpha), \tau, \alpha) = & \int_0^L \frac{1}{2} \varepsilon(u^0(x; \alpha)) E_0 \varepsilon(u^1(x; \alpha)) + \tau(x; \alpha) \varepsilon(u^0(x; \alpha)) - f(x)(u^0(x; \alpha)) \\ & - \frac{1}{2} \int_0^L \tau(x; \alpha) (E(x; \alpha) - E_0)^{-1} \tau(x; \alpha) dx + \int_0^L \frac{1}{2} \tau(x; \alpha) \varepsilon(u^1(x; \alpha)) dx \end{aligned} \quad (3.36)$$

The function $u^0(x)$, defined by Eq.(3.31), can be easily obtained using any appropriate numerical approximation method, see Section 4.3 and 4.4. The determination of $u^1(x; \alpha)$, however, is a little bit more involved. In particular, we employ the Green's function method for solution of this problem.

4.2.3 Green's function method

The Green's function is an exact solution of the partial differential equations, one having an impulse forcing term at a point y , it is the response of the body (with appropriate boundary conditions) to a concentrated energy source. Technically, a Green's function of a linear operator

L at a point x_0 , is any solution of $(Lf)(x) = \delta(x - x_0)$, where δ is the Dirac delta function.¹ Given the GF for a particular geometry, almost any problem can be solved by integration. It is known only for the simplest equations and specific geometries, such as the problem under consideration.

It is shown on an example below, Figure 8, how to derive GF for a given structure. In particular, a simply supported beam is shown in Figure 8(a), a unit force is applied at a given point y in the beam. The distribution of strain is plotted in Figure 8(b)

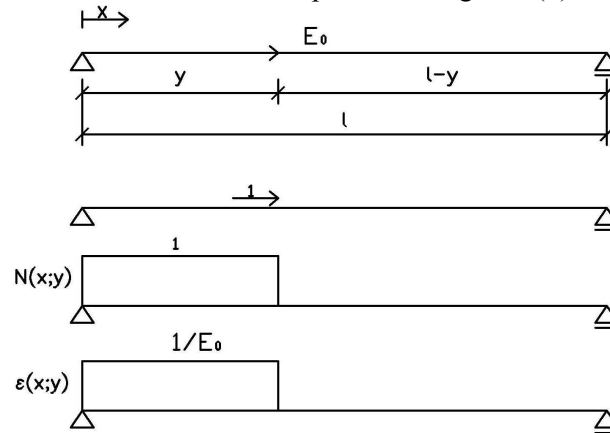


Figure 11 Derivation of the Green's function, (a) geometry, (b) normal forces, (c) strain distribution

Recall that the Green function corresponds to the displacement due to concentrated force at y . From Figure 11, it can be easily seen that displacement field is given by

$$u(x) = G(x, y) = \begin{cases} \frac{x}{E_0} & x \leq y \\ \frac{y}{E_0} & x > y \end{cases}, \quad (3.37)$$

It should be emphasized again, however, that such an analysis can only be performed in very special cases. Generally, one has to resort to a numerical approximation schemes leading to an approximate expression for the Green function $G^h(x, y)$. More details about this procedure can be found in Chapters 5 and 6.

Once the Green's function is available, the strain field results from the equation

$$\frac{d}{dx} \left(E_0 \frac{du^1(x; \alpha)}{dx} + \tau(x; \alpha) \right) = 0 \quad (3.38)$$

¹ The Dirac delta function, sometimes referred to as the unit impulse function and introduced by the British theoretical physicist Paul Dirac, can usually be informally thought of as a function $\delta(x)$ that has the value of infinity for $x = 0$, the value zero elsewhere. The integral from minus infinity to plus infinity is 1.

complemented with the same type of boundary conditions as for function $u_0(x)$, but now we consider the *homogeneous* values (zero displacement or zero stress). After rewriting Eq.(3.38) in the form:

$$\frac{d}{dx}(E_0 \frac{du^1(x;\alpha)}{dx}) + \frac{d}{dx}(\tau(x;\alpha)) = 0,$$

we can obtain function $u^1(x;\alpha)$ using by parts integration,

$$u^1(x;\alpha) = \int_0^L G(x;y) \frac{d}{dy} \tau(y;\alpha) dy = [G(x;y)(\tau(y;\alpha))]_0^L - \int_0^L \frac{\partial G(x;y)}{\partial y} \tau(y;\alpha) dy. \quad (3.39)$$

The term in brackets disappears due to homogeneity of the boundary conditions. Finally, this leads to expression for the strain field due to polarization stress

$$\varepsilon(u^1(x;\alpha)) = \frac{d}{dx} u^1(x;\alpha) = - \int_0^L \frac{\partial^2 G(x;y)}{\partial x \partial y} \tau(y;\alpha) dy = - \int_0^L \Gamma(x;y) \tau(y;\alpha) dy. \quad (3.40)$$

In the real-world application, we replace exact Eq. (3.40) with the approximate version

$$\varepsilon(u^1(x;\alpha)) \approx - \int_0^L \Gamma_h(x;y) \tau(y;\alpha) dy. \quad (3.41)$$

Again, the particular choice of the discretized function Γ_h depends on the selected discretization scheme.

4.2.4 Probabilistic averaging

Using the results of the previous section, we are able to link the unknown strain field $\varepsilon_1(x;\alpha)$ to the polarization stress $\tau(x;\alpha)$, which now becomes the primary variable of the problem. In order to separate effects of the spatial variation and the stochasticity of the response, we introduce a following separable expression of the polarization field

$$\tau(x;\alpha) = \sum_r \tau_r(x) \chi_r(x;\alpha), \quad (3.42)$$

where τ_r denotes *deterministic* value of polarization field related to the r -th phase and χ_r is the characteristic function introduced in Section 3.1.2 Now, we will proceed with considering a stochastic variational principle

$$\max_{\tau} \text{EX}(U(\tau)) = \int_0^L U(\tau;\alpha) p(\alpha) d\alpha, \quad (3.43)$$

In the view of following derivation, we decompose the Hashin-Shtrikman function into three parts, namely

$$U(\tau;\alpha) = \underbrace{\int_0^L \frac{1}{2} \varepsilon(u^0(x)) E_0 \varepsilon(u^0(x)) + \tau(x;\alpha) \varepsilon(u^0(x)) - f(x)(u^0(x)) dx}_{I_1} - \underbrace{\frac{1}{2} \int_0^L \tau(x;\alpha) (E(x;\alpha) - E_0)^{-1} \tau(x;\alpha) dx}_{I_2} + \underbrace{\int_0^L \frac{1}{2} \tau(x;\alpha) \left[- \int_0^L \Gamma_h(x;y) \tau(y;\alpha) dy \right] dx}_{I_3}$$

Performing statistical averaging of integral I_1 yields

$$\begin{aligned}
EX(I_1) &= \int_0^L \int_s \tau_r(x; \alpha) \varepsilon(u^0(x)) dx p(\alpha) d\alpha = \int_0^L \sum_r \int_s \tau_r(x) \chi_r(x; \alpha) \varepsilon(u^0(x)) p(\alpha) d\alpha dx \\
&= \sum_r \int_0^L \tau_r(x) \varepsilon(u^0(x)) c_r(x) dx.
\end{aligned}$$

Treatment of integral I_2 is a little bit more involved. In particular, we get

$$\begin{aligned}
EX(I_2) &= -\frac{1}{2} \int_0^L \int_s \left\{ \sum_r \tau_r(x) \chi_r(x; \alpha) \right\} (E(x; \alpha) - E_0)^{-1} \left\{ \sum_s \tau_s(x) \chi_s(x; \alpha) \right\} dx p(\alpha) d\alpha \\
&= -\frac{1}{2} \int_0^L \sum_r \sum_s \int_s (E(x; \alpha) - E_0)^{-1} \chi_r(x; \alpha) \chi_s(x; \alpha) p(\alpha) d\alpha \tau_r(x) \tau_s(x).
\end{aligned}$$

Taking into account the fact that

$$\chi_r(x; \alpha) \chi_s(x; \alpha) = \delta_{rs} \chi_r(x; \alpha),$$

where δ_{rs} denotes the Kronecker's delta with properties

$$\delta_{rs} = \begin{cases} 1 & \text{if } r=s \\ 0 & \text{if } r \neq s \end{cases},$$

we arrive at the expression

$$\begin{aligned}
EX(I_2) &= -\frac{1}{2} \int_0^L \sum_r \int_s \tau_r(x) (E_r - E_0)^{-1} \tau_r(x) \chi_r(x; \alpha) p(\alpha) d\alpha \\
&= -\frac{1}{2} \sum_r \int_0^L \tau_r(x) c_r(x) \tau_r(x) (E_r - E_0)^{-1}(x) dx.
\end{aligned}$$

Now, we are left with statistical averaging of I_3 . This amounts to computing

$$\begin{aligned}
EX(I_3) &= -\frac{1}{2} \int_0^L \sum_r \tau_r(x) \chi_r(x; \alpha) \int_0^L \Gamma_h(x; y) \sum_s \tau_s(y) \chi_s(y; \alpha) dy dx p(\alpha) d\alpha \\
&= -\frac{1}{2} \int_0^L \int_0^L \left\{ \sum_r \sum_s \int_s \chi_r(x; \alpha) \chi_s(y; \alpha) p(\alpha) d\alpha \right\} \tau_r(x) \Gamma_h(x; y) \tau_s(y) dx dy \\
&= -\frac{1}{2} \sum_r \sum_s \int_0^L \int_0^L S_{rs}(x; y) \tau_r(x) \Gamma_h(x; y) \tau_s(y) dx dy \\
&= -\frac{1}{2} \sum_{r,s} \int_0^L \tau_r(x) \int_0^L S_{rs}(x; y) \Gamma_h(x; y) \tau_s(y) dy dx,
\end{aligned}$$

where S_{rs} is the two-point probability function introduced in Section 3.1.2. Collecting the resulting expressions for integrals I_1 , I_2 and I_3 , we arrive at the statistically averaged approximated Hashin-Shtrikman functional, now expressed solely in terms of phase polarization fields τ_r .

$$\begin{aligned}
EX(U(\tau)) &= \int_0^L \frac{1}{2} \varepsilon(u^0(x)) E_0 \varepsilon(u^0(x)) - f(x)(u^0(x)) dx + \sum_r \int_0^L \tau_r(x) \varepsilon(u^0(x)) c_r(x) dx \\
&\quad - \frac{1}{2} \sum_r \int_0^L \tau_r(x) c_r(x) \tau_r(x) (E_r - E_0)^{-1}(x) dx \\
&\quad - \frac{1}{2} \sum_{r,s} \int_0^L \tau_r(x) \int_0^L S_{rs}(x;y) \Gamma_h(x;y) \tau_s(y) dy dx.
\end{aligned} \tag{3.44}$$

4.2.5 Stationarity conditions

In the last step of the analysis, we perform maximization of Eq. (3.44) with respect to phase polarization field. Stationarity conditions of the approximated Hashin-Shtrikman variational principle attain the form ($i \in \{m, h\}$):

$$\begin{aligned}
\delta\tau_i EX(U(\tau)) &= \int_0^L \delta\tau_i(x) c_r(x) \varepsilon(u^0(x)) dx - \int_0^L \delta\tau_i(x) c_r(x) (E_r - E_0)^{-1} \tau_i(x) dx \\
&\quad - \int_0^L \delta\tau_i(x) \sum_j \int_0^L S_{ij}(x;y) \Gamma_h(x;y) \tau_j(y) dy dx = 0.
\end{aligned} \tag{3.45}$$

Eq. (3.45) still presents an infinite system of conditions to be fulfilled. To reduce these conditions to a finite-dimensional problem, a proper discretization scheme needs to be set up. This topic is covered in the following two chapters.

5 Finite element method

5.1 Introduction

Generally speaking, FEM is a numerical technique for a boundary value problem. In its application, the object or system is represented by a geometrically similar model consisting of multiple, linked, simplified representations of discrete regions, i.e., finite elements. Equations of equilibrium, in conjunction with applicable physical considerations such as compatibility and constitutive relations, are applied to each element, and a system of simultaneous equations is constructed. The system of equations is solved for unknown values using the techniques of linear algebra or nonlinear numerical schemes, as appropriate. While being an approximate method, the accuracy of the FEM method can be improved by refining the mesh in the model using more elements and nodes. In the next sections, it is shown how to apply the FEM for solving the Hashin-Shtrikman problem.

5.2 Solution $u^0(x)$

The solution of the homogeneous problem follows the standard finite element procedures, see, e.g. [5]. Nevertheless, we briefly repeat the basic steps of the method for the sake of clarity. The FEM starts with the condition for a weak solution, defined via variational statement (3.45)

$$\int_0^L \varepsilon(\delta v(x)) E_0 \varepsilon(u^0(x)) - \delta v(x) f(x) dx - \delta v(L) F = 0, \quad (3.46)$$

which should be satisfied for any kinematically admissible test function δv . Within the standard FEM framework, the structure is discretized in n intervals of length $h = L/n$ and $(n+1)$ nodal points. The unknown displacement field u^0 as well as test function δv together with their derivatives are approximated as

$$\begin{aligned} u(x) &\approx \mathbf{N}_u(x) \mathbf{r}_u, & \delta v(x) &\approx \mathbf{N}_u(x) \delta \mathbf{r}_u, \\ \varepsilon(u(x)) &\approx \mathbf{B}_u(x) \mathbf{r}_u, & \varepsilon(\delta v(x)) &\approx \mathbf{B}_u(x) \delta \mathbf{r}_u, \end{aligned} \quad (3.47)$$

where $\mathbf{N}(x)$ is a row matrix of piecewise linear basis functions, $\mathbf{B}(x)$ is the geometric matrix relating nodal displacements \mathbf{r}_u to strains. Inserting (3.47) into (3.46) yields

$$\delta \mathbf{r}_u^T \mathbf{K}_u \mathbf{r}_u = \delta \mathbf{r}_u^T (\mathbf{R}_f + \mathbf{R}_F),$$

where the stiffness matrix and vector of equivalent nodal forces have the familiar form

$$\begin{aligned} \mathbf{K}_u &= \int_0^L \mathbf{B}_u^T(x) E_0 \mathbf{B}_u(x) dx, \\ \mathbf{R}_f &= \int_0^L \mathbf{N}_u^T(x) f(x) dx, \\ \mathbf{R}_F &= \mathbf{N}_u^T(L) F. \end{aligned} \quad (3.48)$$

By arbitrariness of $\delta \mathbf{r}_u$, we finally obtain the system of linear equations

$$\mathbf{K}_u \mathbf{r}_u = \mathbf{R}_u, \quad (3.49)$$

which allows us to finally obtain the approximation for displacement field. Note that the stiffness matrix \mathbf{K}_u is *symmetric* and *sparse*.

5.3 Function Γ^h

Recall that application of Hashin-Shtrikman method needs an estimation of the Green's function of the problem. Recall that the Green's function corresponds to a displacement field at x for a unit force applied at a point y . It follows from Eq. (3.49) that the nodal displacements for this loading satisfy the condition

$$\mathbf{K}_u \mathbf{r}_u = \mathbf{N}_u^T(y) 1$$

and hence the discretized Green's function is provided by relation

$$G_u^h(x, y) = \mathbf{N}_u(x) \mathbf{K}_u^{-1} \mathbf{N}_u^T(y). \quad (3.50)$$

Now we can easily obtain the relation for (negative value) of displacement field due to polarization by replacing the partial derivative with respect to y in Eq. (3.39) with the multiplication by the \mathbf{B}_u matrix

$$\Gamma_u^h(x, y) = \mathbf{N}_u(x) \mathbf{K}_u^{-1} \mathbf{B}_u^T(y). \quad (3.51)$$

Repeating the same argument for Eq. (3.40) leads to the final expression

$$\Gamma_h(x, y) = \mathbf{B}_u(x) \mathbf{K}_u^{-1} \mathbf{B}_u^T(y). \quad (3.52)$$

Note that for the adopted piecewise linear basis function the matrix function $\mathbf{B}_u(y)$ is piecewise

constant on each element $e=1, 2, \dots, n$. Due to this fact, it suffices to “sample” functions (3.51) and (3.52) on a set of integration points ξ_e , $e=1, 2, \dots, n$, each located in the center of each element. The examples of these functions are shown in the following figure for different parameters h .

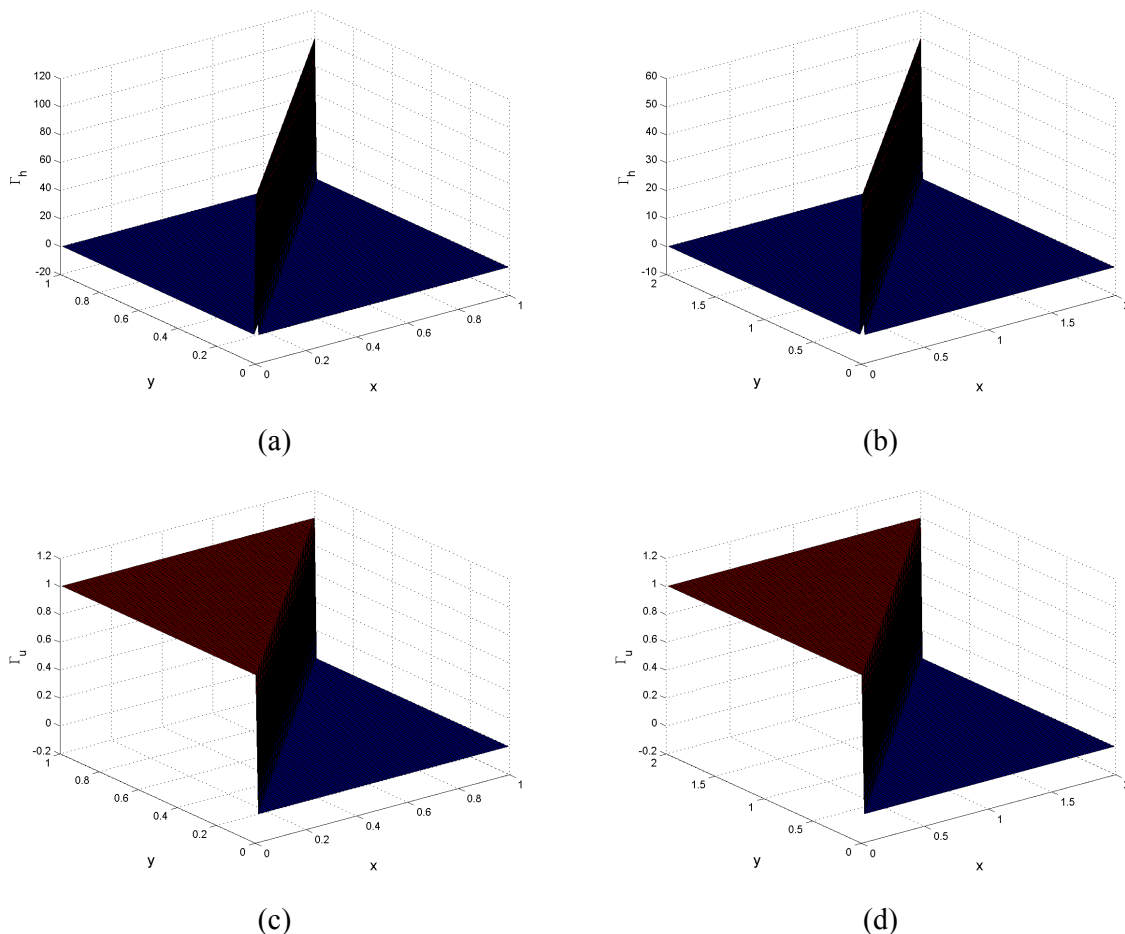


Figure 12 Examples of displacement and strain Green's function approximated by FEM
(a,b) Function I^h , (c,d) F^u . Mesh parameters are $n=120, h=0.2$ and $n=60, h=0.5$, respectively,
 $E_0=1 \text{ Pa}, L=1 \text{ m}$

Comparing these approximations with the analytical formulas(3.37), we see that the FEM provides indeed a very reasonable approximation for the exact Green's function within the limitation imposed by a finite mesh size h (observe changes in the magnitude in Figure 12(a,b)).

5.4 Solution of the polarization problem

Having solved the auxiliary problem and determined an appropriate expression, we are left with the unknown phase polarization stresses τ_r . Recall that this quantity follows from stationarity conditions

$$\begin{aligned}
0 = & \int_0^L \delta\tau_i(x)c_r(x)\varepsilon(u^0(x))dx - \int_0^L \delta\tau_i(x)c_r(x)(E_r - E_0)^{-1}\tau_i(x)dx \\
& - \int_0^L \delta\tau_i(x) \sum_j \int_0^L S_{ij}(x;y)\Gamma_h(x;y)\tau_j(x)dydx
\end{aligned} \tag{3.53}$$

To this end, we introduce an approximation of polarization stresses and corresponding weight functions in the form

$$\tau_i(x) \approx \mathbf{N}_\tau(x)\mathbf{r}_\tau^i, \quad \delta\tau_i(x) \approx \mathbf{N}_\tau(x)\delta\mathbf{r}_\tau^i. \tag{3.54}$$

Notice that because the unknown polarization field appears only in the 0-th derivative in Eq. (3.53), it suffices to select piecewise constant basis functions \mathbf{N}_τ . Then, the vector of unknowns \mathbf{r}_τ^i has the physical meaning of polarization stress related to the phase i at integration points ξ_e within the structure. The stationarity conditions (3.53) can now have a particular form

$$(\delta\mathbf{r}_\tau^i)^T \mathbf{K}_\tau^i \mathbf{r}_\tau^i + (\delta\mathbf{r}_\tau^i)^T \sum_j \mathbf{K}_\tau^{ij} \mathbf{r}_\tau^j = (\delta\mathbf{r}_\tau^i)^T \mathbf{R}_\varepsilon^i, \tag{3.55}$$

where the individual matrices are defined as

$$\begin{aligned}
\mathbf{K}_\tau^i &= \int_0^L \mathbf{N}_\tau^T(x)c_i(x)(E_i - E_0)^{-1}\mathbf{N}_\tau(x)dx, \\
\mathbf{K}_\tau^{ij} &= \int_0^L \int_0^L \mathbf{N}_\tau^T(x)\Gamma_h(x;y)S_{ij}(x;y)\mathbf{N}_\tau(y)dxdy, \\
\mathbf{R}_\varepsilon^i &= \int_0^L \mathbf{N}_\tau^T(x)c_i(x)\varepsilon^0(x)dx.
\end{aligned} \tag{3.56}$$

By arbitrariness of $\delta\mathbf{r}_\tau^i$, we obtain that for a two-phase media (with an obvious generalization for multi-phase materials) the condition (3.55) is equivalent to the system

$$\begin{bmatrix} \mathbf{K}_\tau^1 + \mathbf{K}_\tau^{11} & \mathbf{K}_\tau^{12} \\ \mathbf{K}_\tau^{21} & \mathbf{K}_\tau^2 + \mathbf{K}_\tau^{22} \end{bmatrix} \begin{Bmatrix} \mathbf{r}_\tau^1 \\ \mathbf{r}_\tau^2 \end{Bmatrix} = \begin{Bmatrix} \mathbf{R}_\varepsilon^1 \\ \mathbf{R}_\varepsilon^2 \end{Bmatrix}, \tag{3.57}$$

which will shortly be denoted as

$$\mathbf{K}_\tau \mathbf{r}_\tau = \mathbf{R}_\varepsilon. \tag{3.58}$$

It can be easily deduced from properties of Γ_h and S_{ij} that it holds, that $\mathbf{K}_\tau^{12} = (\mathbf{K}_\tau^{21})^T$. Hence, the stiffness matrix \mathbf{K}_τ is symmetric *dense* $n \times n$ matrix, which is negative definite provided that $E_0 < \min(E_i)$; see, e.g., [6] for a rigorous proof. Solving system (3.58) allows us to obtain phase polarization stresses at individual integration points.

Recall that for the adopted discretization (u^0 linear, τ_i piecewise constant), the individual terms up to S_{ij} and c_i are piecewise constant on each element e . Hence, it appears to be reasonable to approximate integrals using one-point quadrature rule. The individual terms in (3.56) have the form

$$\begin{aligned}
\mathbf{K}_\tau^i &\approx h \sum_e \mathbf{N}_\tau^T(\xi_e) c_i(\xi_e) (E_i - E_0)^{-1} \mathbf{N}_\tau(\xi_e), \\
\mathbf{K}_\tau^{ij} &\approx h^2 \sum_e \sum_{e'} \mathbf{N}_\tau^T(\xi_e) \Gamma_h(\xi_e; \xi_{e'}) S_{ij}(\xi_e; \xi_{e'}) \mathbf{N}_\tau(\xi_{e'}), \\
\mathbf{R}_\varepsilon^i &\approx h \sum_e \mathbf{N}_\tau^T(\xi_e) c_i(\xi_e) \varepsilon^0(\xi_e).
\end{aligned} \tag{3.59}$$

Note that the approximations in Eq. (3.59) are exact when the variation of S_{ij} and c_i is linear. However, this is not the case of the adopted microstructural model and hence this step certainly introduces additional error into the solution.

5.5 Results postprocessing

The last step of any numerical scheme is determination of the resulting quantities of interest. In our context, this means determination of expected values of displacements $\text{EX}(u)$, strains $\text{EX}(\varepsilon)$ and stresses $\text{EX}(\sigma)$. Nevertheless, as the first step, the expected value of the polarization field is obtained at individual integration points

$$\text{EX}(\tau(x)) = \mathbf{N}_\tau(x) \text{EX}(\mathbf{r}_\tau) = \mathbf{N}_\tau(x) \sum_i c^i(x) \mathbf{r}_\tau^i, \tag{3.60}$$

Now we can evaluate the expected value of displacement field using already derived function Γ_u^h , recall Eq. (3.51),

$$\begin{aligned}
\text{EX}(u(x)) &\approx u^0(x) - \int_0^L \Gamma_u^h(x, y) \text{EX}(\tau(y)) dy \\
&= \mathbf{N}_u(x) \mathbf{r}_u - \int_0^L \mathbf{N}_u(x) \mathbf{K}_u^{-1} \mathbf{B}_u^T(y) \mathbf{N}_\tau(y) dy \text{EX}(\mathbf{r}_\tau) \\
&= \mathbf{N}_u(x) \left(\mathbf{r}_u - \int_0^L \mathbf{N}_u(x) \mathbf{K}_u^{-1} \mathbf{B}_u^T(y) \mathbf{N}_\tau(y) \text{EX}(\mathbf{r}_\tau) \right) \\
&= \mathbf{N}_u(x) \text{EX}(\mathbf{r}_u).
\end{aligned} \tag{3.61}$$

For the introduced discretization scheme, the expected value on nodal displacement $\text{EX}(\mathbf{r}_u)$ can be obtained using the one-point quadrature

$$\text{EX}(\mathbf{r}_u) \approx \mathbf{r}_u - h \left(\sum_e \mathbf{K}_u^{-1} \mathbf{B}_u^T(\xi_e) \mathbf{N}_\tau(\xi_e) \right) \text{EX}(\mathbf{r}_\tau). \tag{3.62}$$

Having established the expected value of nodal displacement, remaining steps are straightforward. Strain field can be directly obtained from previous equation as

$$\text{EX}(\varepsilon(x)) \approx \mathbf{B}_u(x) \text{EX}(\mathbf{r}_u) \tag{3.63}$$

and the stress field can be computed as

$$\text{EX}(\sigma(x)) = E_0 \text{EX}(\varepsilon(x)) + \text{EX}(\tau(x)). \tag{3.64}$$

This is actually the last step of the FEM-Hashin-Shtrikman approximation method.

5.6 Algorithmic details of FEM-Hashin-Shtrikman solution

The whole algorithm introduced in this chapter can be summarized in the following steps:

Step 1 – Initialization :

- Divide the structure into n finite elements of length h
- Generate nodal and integration points for each element

Step 2 – Solution of homogenous problem:

- Assemble the local stiffness matrix \mathbf{K}_u for each element
- Construct the global stiffness matrix \mathbf{K}_u by localization according to Eq.(3.48)
- Assemble the vector of nodal loading \mathbf{R}_u according to Eq.(3.48)
- Solve the equilibrium equation $\mathbf{K}_u \mathbf{r}_u = \mathbf{R}_u$ and get the displacement vector \mathbf{r}_u according to Eq.(3.49)
- Compute strain-displacement transformation matrix \mathbf{B}_u
- Evaluate strain $\varepsilon = \mathbf{B}_u \mathbf{r}_u$ approximated by Eq.(3.47)
- Solve system: $\mathbf{K}_u \Gamma_u = \mathbf{B}_u$ according to Eq.(3.51)
- Get discrete Green's function: $\Gamma_h = \mathbf{B}_u^T \Gamma_u$ according to Eq.(3.52)

Step 3 – Geometry analysis:

- Compute local volume fraction at any point x according to Eq.(3.18)
- Calculate two point probability function S_{mm} according to Eq.(3.15)

Step 4 – Hashin-Shtrikman approximation:

- Solution to the polarization problem: $\mathbf{K}_\tau \mathbf{r}_\tau = \mathbf{R}_\tau$ according to Eq.(3.57)
- Use approximation $\tau_i(x) \approx \underline{\mathbf{N}}_\tau(x) \mathbf{r}_\tau^i$

Step 5 – Post processing of results:

- Evaluate the expectation values for the displacement, stress and strain according to Eq.(3.60),(3.61),(3.63) and (3.64)
- Plot the graphs

We refer an interested reader to Section 10.2 for a more concrete implementation of individual steps.

6 Boundary element method

6.1 BEM introduction

Boundary Element Methods (BEM) is a very powerful numerical method which can solve complex problems in a wide variety of engineering disciplines, e.g. fluid mechanics, solid and fracture mechanics, acoustics, etc. The boundary (rather than the volume) of a domain is discretized into panels on which the related quantities (e.g. velocity potential, displacements and tractions, acoustic, temperature, etc) are approximated with distributions of known shape but of unknown strength. The unknown strengths are determined by applying the specified boundary conditions, and by solving an integral equation (e.g. Green's identity) over the boundary.

In BEM, the structure is divided into infinite bodies and the equations contain only boundary

integrals (and no domain integrals as in Finite Elements) It relates the value of u at some point inside the solution domain to integral expressions involving u and $\frac{\partial u}{\partial n}$ over the boundary of the solution domain. Rather than having an expression relating the value of u at some point inside the domain to boundary integrals, a more useful expression would be one relating the value of u at some point on the boundary to boundary integrals.

Before one applies the boundary element method to a particular problem one must obtain a *fundamental solution* (which is similar to the idea of a particular solution in ordinary differential equations and is the weighting function). Fundamental solutions are attached to the Dirac delta function. The fundamental solution of a particular equation is the weighting function that is used in the boundary element formulation of that equation.

These principles are illustrated in detail in the following text. However, since the BEM is not so frequently used in civil engineering, we slightly depart from the analysis presented in Chapter 5 and present a detailed treatment the stochastic problem within the framework of boundary integral equations (BIE) in Section 6.2. Then, we quickly proceed in the spirit of FEM-based analysis, recovering the solution of the homogeneous problem, finite body Green's function approximation, solution of the polarization problem and postprocessing of the results. The chapter is concluded with algorithmic scheme of BEM-Hashin-Shtrikman method.

6.2 BEM approximation in one dimension

6.2.1 Infinite body Green's function

Unlike FEM, which uses identical approximation for the unknown variable as well as weight function, BEM builds on a solution for infinite body, defined from $-\infty$ to $+\infty$. This function is generally available for more-dimensional geometries, see, e.g. [5],[7]. It is defined exactly in the same way as for the finite-body case, see Section 4.2.3.,

$$E_0 \frac{\partial^2 G(x; y)}{\partial x^2} + \delta(y) = 0. \quad (3.65)$$

Observe that now, however, the Green's function must be transitionally invariant due to infiniteness of the body. It can be rather easily seen that the one-dimensional Green's function satisfying the translation invariance has the form

$$E_0 G^\infty(x; y) = -\frac{1}{2}|x - y|. \quad (3.66)$$

In the subsequent derivations, we will utilize the following partial derivatives:

$$E_0 \frac{\partial G^\infty(x; y)}{\partial x} = H(y - x) - \frac{1}{2}, \quad E_0 \frac{\partial G^\infty(x; y)}{\partial y} = -H(y - x) + \frac{1}{2}, \quad (3.67)$$

$$E_0 \frac{\partial^2 G^\infty(x; y)}{\partial x^2} = -\delta(y), \quad E_0 \frac{\partial^2 G^\infty(x; y)}{\partial x \partial y} = \delta(y), \quad (3.68)$$

where H is the Heaviside step function (the Dirac delta function is the slope of the Heaviside step function).

$$H(x) = \begin{cases} 1 & x > 0 \\ 0 & x < 0 \end{cases}.$$

6.2.2 General relations

Recall that the following ordinary differential equation (ODE) with constant coefficients needs to be solved (equilibrium condition):

$$\frac{d}{dx} \left(E_0 \frac{du(x; \alpha)}{dx} + \tau(x; \alpha) \right) + f(x) = 0$$

plus the boundary conditions

$$u(0; \alpha) = 0,$$

$$E_0 \frac{du(L; \alpha)}{dx} + \tau(L; \alpha) = R(L; \alpha) = F.$$

The BEM method starts from the notion of *very weak solution*, which basically follows from applying twice *per partes* integration to the following identity (weak solution):

$$\int_0^L v(x) \frac{d}{dx} \left(E_0 \frac{du(x; \alpha)}{dx} + \tau(x; \alpha) \right) dx + \int_0^L v(x) f(x) dx = 0$$

After the first by-part integration it results:

$$[v(x)R(x; \alpha)]_0^L - \int_0^L \frac{dv(x)}{dx} \left(E_0 \frac{du(x; \alpha)}{dx} + \tau(x; \alpha) \right) dx + \int_0^L v(x) f(x) dx = 0$$

After the second by-parts integration:

$$[v(x)R(x; \alpha)]_0^L - \int_0^L \frac{dv(x)}{dx} \tau(x; \alpha) dx - \left[\frac{dv(x)}{dx} E_0 u(x; \alpha) \right]_0^L + \int_0^L \frac{d^2 v(x)}{dx^2} E_0 u(x; \alpha) dx + \int_0^L v(x) f(x) dx = 0$$

The test function $v(x)$ is selected in the particular form (assume that y is arbitrary but fixed for each realization):

$$v(x) = G^\infty(x; y)$$

By inserting the test function into the previous equation we obtain the identity:

$$\begin{aligned} & [G(x; y)R(x; \alpha)]_0^L - \int_0^L \frac{\partial G(x; y)}{\partial x} \tau(x; \alpha) dx - \left[\frac{\partial G(x; y)}{\partial x} E_0 u(x; \alpha) \right]_0^L + \int_0^L \frac{\partial^2 G(x; y)}{\partial x^2} E_0 u(x; \alpha) dx \\ & + \int_0^L G(x; y) f(x) dx = 0 \end{aligned}$$

Hence the displacement at any point $y \in (0, L)$ follows from:

$$u(x; \alpha) = [G(x; y)R(x; \alpha)]_0^L - \int_0^L \frac{\partial G(x; y)}{\partial x} \tau(x; \alpha) dx - \left[\frac{\partial G(x; y)}{\partial x} E_0 u(x; \alpha) \right]_0^L + \int_0^L G(x; y) f(x) dx$$

Inserting the relations(3.67), (3.68) into the previous equation leads to

$$\begin{aligned}
u(y; \alpha) = & \left[-\frac{1}{2} \frac{|x-y|}{E_0} R(x; \alpha) \right]_0^L - \int_0^L \frac{1}{E_0} \left(H(y-x) - \frac{1}{2} \right) \tau(x; \alpha) dx \\
& - \left[\left(H(y-x) - \frac{1}{2} \right) u(x; \alpha) \right]_0^L + \int_0^L -\frac{1}{2} \frac{|x-y|}{E_0} f(x) dx
\end{aligned} \tag{3.69}$$

In the following computation, a value of strain ε at any point needs to be evaluated. It follows from general expression

$$\begin{aligned}
\frac{du(y; \alpha)}{dy} = & \left[\frac{\partial G(x; y)}{\partial y} R(x; \alpha) \right]_0^L - \int_0^L \frac{\partial G^2(x; y)}{\partial x \partial y} \tau(x; \alpha) dx - \left[\frac{\partial G^2(x; y)}{\partial x \partial y} E_0 u(x; \alpha) \right]_0^L \\
& + \int_0^L \frac{\partial G(x; y)}{\partial y} f(x) dx
\end{aligned}$$

which, when specialized for the particular Green's function, reduces to

$$\begin{aligned}
\varepsilon(y; \alpha) = & \left[\frac{1}{E_0} \left(\frac{1}{2} - H(y-x) \right) R(x; \alpha) \right]_0^L - \int_0^L \frac{1}{E_0} \delta(y) \tau(x; \alpha) dx - \left[\delta(y) u(x; \alpha) \right]_0^L \\
& + \int_0^L \frac{1}{E_0} \left(\frac{1}{2} - H(y-x) \right) f(x) dx \\
= & \frac{1}{2E_0} (R(0; \alpha) + R(L; \alpha)) - \frac{1}{E_0} \tau(x; \alpha) + \frac{1}{2E_0} \left(\int_0^y f(x) dx - \int_y^L f(x) dx \right)
\end{aligned} \tag{3.70}$$

Note that both relations for strain and displacement field are explicit, once the boundary data $u(0; \alpha)$, $u(L; \alpha)$, $R(0; \alpha)$ and $R(L; \alpha)$ are specified, provided that it is assumed that polarization stress τ is given. From these mentioned quantities, two are always specified due to geometry and boundary conditions. The remaining two are obtained from the boundary equations (3.69) for $y \rightarrow 0_+$ and $y \rightarrow L_-$.

While y approaches the boundary, care should be taken in order to treat the Heaviside function correctly, due to the different boundary conditions. Therefore, the passage is done in two separate steps:

For $y \rightarrow 0_+$

$$\begin{aligned}
u(0, \alpha) = & -\frac{1}{2E_0} \left[|x-0| R(x; \alpha) \right]_0^L - \frac{1}{E_0} \int_0^L \left(H(0-x) - \frac{1}{2} \right) \tau(x; \alpha) dx - \left[\left(H(0_+ - x) - \frac{1}{2} \right) u(x; \alpha) \right]_0^L \\
& - \frac{1}{2E_0} \int_0^L |x-0| f(x) dx \\
= & -\frac{1}{2E_0} LR(L; \alpha) + \frac{1}{2E_0} \int_0^L \tau(x; \alpha) dx + \frac{1}{2} (u(0; \alpha) + u(L; \alpha)) - \frac{1}{2E_0} \int_0^L xf(x) dx
\end{aligned}$$

Similarly, for $y \rightarrow L_-$, we obtain:

$$\begin{aligned}
u(0, \alpha) &= -\frac{1}{2E_0} \left[|x-L| R(x; \alpha) \right]_0^L - \frac{1}{E_0} \int_0^L \left(H(L-x) - \frac{1}{2} \right) \tau(x; \alpha) dx - \left[\left(H(L-x) - \frac{1}{2} \right) u(x; \alpha) \right]_0^L \\
&\quad - \frac{1}{2E_0} \int_0^L |x-L| f(x) dx \\
&= -\frac{1}{2E_0} LR(L; \alpha) + \frac{1}{2E_0} \int_0^L \tau(x; \alpha) dx + \frac{1}{2} (u(0; \alpha) + u(L; \alpha)) + \frac{1}{2E_0} \int_0^L (x-L) f(x) dx,
\end{aligned}$$

In overall, the boundary data must satisfy the following system of linear equations:

$$E_0 u(0; \alpha) - E_0 u(L; \alpha) + LR(L; \alpha) = \int_0^L \tau(x; \alpha) dx - \int_0^L x f(x) dx \quad (3.71)$$

$$-E_0 u(0; \alpha) + E_0 u(L; \alpha) - LR(0; \alpha) = -\int_0^L \tau(x; \alpha) dx + \int_0^L (x-L) f(x) dx \quad (3.72)$$

As for the finite element discretization, the problem is divided into two steps; deterministic and stochastic part; and solved separately. Details on solution of individual steps are presented in the following two subsections.

6.3 Solution $u^0(x)$

Recall that the solution u^0 corresponds to the original problem with $\tau=0$ Pa and “real” boundary conditions. Therefore, the system of equations(3.71),(3.72) has the form:

$$\begin{aligned}
E_0 u^0(0) - E_0 u^0(L) + LR^0(L) &= -\int_0^L x f(x) dx, \\
-E_0 u^0(0) + E_0 u^0(L) - LR^0(0) &= \int_0^L (x-L) f(x) dx,
\end{aligned} \quad (3.73)$$

which can be used to determine all the boundary quantities. Once these values are obtained, the displacement at any internal point of the structure follows from the expression below, see Eq.(3.69)

$$u^0(y) = \left[-\frac{1}{2E_0} |x-y| R^0(x) \right]_0^L - \left[\left(H(y-x) - \frac{1}{2} \right) u^0(x) \right]_0^L - \int_0^L \frac{1}{2E_0} |x-y| f(x) dx \quad (3.74)$$

and the strain ε^0 follows from

$$\varepsilon^0(y) = \frac{1}{2E_0} (R^0(0) + R^0(L)) + \frac{1}{2E_0} \left(\int_0^y f(x) dx - \int_y^L f(x) dx \right). \quad (3.75)$$

6.4 Solution $u^1(x; \alpha)$

The solution $u^1(x; \alpha)$ corresponds to the solution of the original problem with zero distributed loading ($f(x) \equiv 0$) and with zero prescribed boundary data ($F=0$ N). The BEI for this case has the

form:

$$E_0 u^1(0; \alpha) - E_0 u^1(L; \alpha) + LR^1(L; \alpha) = \int_0^L \tau(x; \alpha) dx, \quad (3.76)$$

$$-E_0 u^1(L; \alpha) + E_0 u^1(0; \alpha) - LR^1(0; \alpha) = -\int_0^L \tau(x; \alpha) dx \quad (3.77)$$

Once the data are determined for a realization α , the strain at any point $y \in (0, L)$ follows from

$$\varepsilon^1(y; \alpha) = \frac{1}{2E_0} (R^1(0; \alpha) + R^1(L; \alpha)) - \frac{1}{E_0} \tau(x; \alpha) \quad (3.78)$$

Recall that the application of the Hashin-Shtrikman principles builds upon relation of strains and polarization stresses via

$$\varepsilon^1(y; \alpha) = -\int_0^L \Gamma^h(y, x) \tau(x; \alpha) dx$$

It follows from the second term in Eq. (3.78) that in the BEM discretization, the Γ^h function contains the following Γ^∞ for the finite body. The first term then takes into account the finite dimension of the analyzed domain. The additional term can be obtained as follows. First, the auxiliary problem of Eq(3.76),(3.77) is solved with the special right hand side,

$$\begin{aligned} E_0 \bar{u}^1(0) - E_0 \bar{u}^1(L) + L\bar{R}^1(L) &= 1 \\ -E_0 \bar{u}^1(0) + E_0 \bar{u}^1(L) - L\bar{R}^1(0) &= -1 \end{aligned}$$

and compute an auxiliary variable as

$$\bar{\Gamma} = \frac{1}{2E_0} (\bar{R}^1(0) + \bar{R}^1(L)) \quad (3.79)$$

Then Eq.(3.78) can be written as

$$\varepsilon^1(y; \alpha) = \bar{\Gamma} \int_0^L \tau(x; \alpha) dx - \frac{1}{E_0} \tau(y; \alpha) = -\int_0^L \left(\frac{1}{E_0} \delta(y) - \bar{\Gamma} \right) \tau(x; \alpha) dx$$

and identify the (BE approximation) to the finite body Green's function as

$$\Gamma^h(x, y) = \frac{1}{E_0} \delta(y) - \bar{\Gamma}. \quad (3.80)$$

Note that for the present statically determinate case, $\bar{\Gamma} = 0$ and the BEM gives the exact solution. This basically completes the BEM approach to discretization of Hashin-Shtrikman variational principles. Indeed, note that when an identical discretization of polarization stress τ is employed

$$\tau^i(x) \approx \mathbf{N}_\tau(x) \mathbf{r}_\tau^i$$

the only terms which differ from the FEM approximation, see Eq. (3.56), are matrices \mathbf{K}_τ^{ij} . They now have the form

$$\begin{aligned}
\mathbf{K}_\tau^{ij} &= \int_0^L \int_0^L \mathbf{N}_\tau^T(x) \Gamma_h(x; y) S_{ij}(x; y) \mathbf{N}_\tau(y) dx dy \\
&= \int_0^L \int_0^L \mathbf{N}_\tau^T(x) \left(\frac{1}{E_0} \delta(x-y) - \bar{\Gamma} \right) S_{ij}(x; y) \mathbf{N}_\tau(y) dx dy \\
&= \int_0^L \mathbf{N}_\tau^T(x) \frac{1}{E_0} S_{ij}(x; x) \mathbf{N}_\tau(x) dx - \bar{\Gamma} \int_0^L \int_0^L \mathbf{N}_\tau^T(x) S_{ij}(x; y) \mathbf{N}_\tau(y) dx dy \\
&= \int_0^L \mathbf{N}_\tau^T(x) \frac{c_i(x) \delta_{ij}}{E_0} \mathbf{N}_\tau(x) dx - \bar{\Gamma} \int_0^L \int_0^L \mathbf{N}_\tau^T(x) S_{ij}(x; y) \mathbf{N}_\tau(y) dx dy.
\end{aligned} \tag{3.81}$$

The one-point-quadrature approximation to submatrices is now given by

$$\mathbf{K}_\tau^{ij} \approx h \sum_e \mathbf{N}_\tau^T(\xi_e) \frac{c_i(\xi_e) \delta_{ij}}{E_0} \mathbf{N}_\tau(\xi_e) - \bar{\Gamma} h^2 \sum_e \sum_{e'} \mathbf{N}_\tau^T(\xi_e) S_{ij}(\xi_e; \xi_{e'}) \mathbf{N}_\tau(\xi_{e'}). \tag{3.82}$$

The rest of the solution procedure exactly duplicates the one presented in Section 5.4.

6.5 Post-processing results

Once the values of polarization stresses are obtained from stationarity conditions of Hashin-Shtrikman variational principles, the expected values of boundary data follows from the statistically averaged form of local boundary equations (3.76), (3.77)

$$E_0 EX(u^1(0)) - E_0 EX(u^1(L)) + L \cdot EX(R^1(L)) = \int_0^L EX(\tau(x)) dx, \tag{3.83}$$

$$-E_0 EX(u^1(0)) + E_0 EX(u^1(L)) - L \cdot EX(R^1(0)) = -\int_0^L EX(\tau(x)) dx, \tag{3.84}$$

where

$$EX(\tau(x)) = \sum_i c_i(x) \tau^i(x)$$

Hence the expected value of the displacement field follows from Eq. (3.69) as

$$\begin{aligned}
EX(u^1(y)) &= - \left[\frac{1}{2E_0} |x-y| EX(R^1(x)) \right]_0^L - \frac{1}{E_0} \int_0^L \left(H(y-x) - \frac{1}{2} \right) EX(\tau(x)) dx \\
&\quad - \left[\left(H(y-x) - \frac{1}{2} \right) EX(u^1(x)) \right]_0^L \\
&= - \left[\frac{1}{2E_0} |x-y| EX(R^1(x)) \right]_0^L - \frac{1}{2} (EX(u^1(0)) + EX(u^1(L))) \\
&\quad - \frac{1}{2E_0} \left(\int_0^y EX(\tau(x)) dx - \int_y^L EX(\tau(x)) dx \right)
\end{aligned} \tag{3.85}$$

Expected value of strain field follows directly from (3.70)

$$\text{EX}(\varepsilon^1(y)) = \frac{1}{2E_0} \left(\text{EX}(R^1(0)) + \text{EX}(R^1(L)) \right) - \frac{1}{E_0} \text{EX}(\tau(x)). \quad (3.86)$$

Once the expected values of fields due to polarization are determined, we can apply the superposition principle to get

$$\begin{aligned} \text{EX}(u(x)) &= u^0(x) + \text{EX}(u^1(x)), \\ \text{EX}(\varepsilon(x)) &= \varepsilon^0(x) + \text{EX}(\varepsilon^1(x)), \\ \text{EX}(\sigma(x)) &= E_0 \text{EX}(\varepsilon(x)) + \text{EX}(\tau(x)). \end{aligned} \quad (3.87)$$

6.6 Algorithmic details of BEM-Hashin-Shtrikman solution

Step 1 – Initialization :

- Define integration points ξ on the intervals $(0, L)$ and nodal points x

Step 2 – Solution of homogenous problem:

- Assemble the stiffness matrix \mathbf{K}_u according to Eq. (3.73)
- Assemble the right hand side \mathbf{R}_u according to Eq. (3.73)
- Solve the system $\mathbf{K}_u \mathbf{r}_u = \mathbf{R}_u$ and get deterministic values of the displacement at nodal points x according to Eq.(3.74)
- get deterministic strains at points ξ according to Eq.(3.75)
- Evaluate I_r (a constant value added to the Green's function for the infinite body) (by solving again the system: $r_\theta = K/R$) according to Eq.(3.79).

Step 3 – Geometry analysis:

- Compute local volume fraction c_m at any point x according to Eq.(3.18)
- Calculate two point probability function S_{mm} according to Eq.(3.15)

Step 4 – Hashin-Shtrikman approximation:

- Assemble the stiffness matrix \mathbf{K}_τ according to Eq.(3.82)
- Solution to the polarization problem: $\mathbf{K}_\tau \mathbf{r}_\tau = \mathbf{R}_\tau$ according to Eq.(3.57)
- Use approximation $\tau_i(x) \approx \underline{\mathbf{N}}_\tau(x) \mathbf{r}_\tau^i$

Step 5 – Post processing of results:

- Evaluate the expectation values for the displacement, stress and strain according to Eq.(3.87)
- Plot the graphs

7 Numerical examples

The first structure studied, is a 1D rod of length L , with left end clamped and free right end. The structure has Young's modulus $E(x, \alpha)$ and is discretized into n linear finite elements (of size h) for the finite element method-based analysis. Two different load cases are studied by both FEM and BEM approach and a comparison is made:

- a) subjected to a uniform loading with intensity $f = 1 \text{ Nm}^{-1}$

b) subjected to applied force $F=1N$ at the right end

For each method and loadcase, we plot the distribution of expected values of displacement $EX(u(x))$, strains $EX(\varepsilon(x))$, stresses $EX(\sigma(x))$ and polarization stresses $EX(\tau(x))$ are shown below. The performance of a given method methods are shown by plotting the graph convergence of the displacement for $x=L$ of the numerical solution to the exact one. An investigation is also made on the rate of the convergence of the method FEM influenced by two factors:

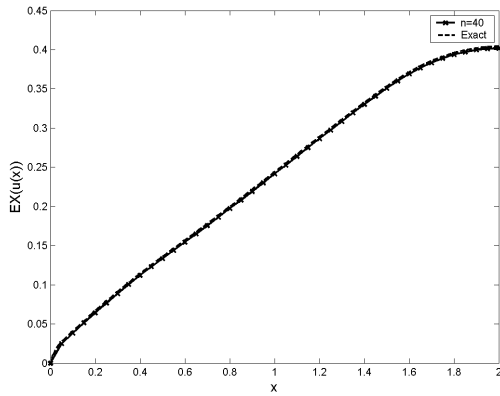
- ratio of E_m/E_h
- size of microstructure l .

For the sake of completeness, an example for a material with uniform intensity (i.e. $\rho_a=\rho_b$) is also presented. Again, we refer an interested reader to Sections 10.2 and 10.3 for more details about the actual implementation of the algorithms.

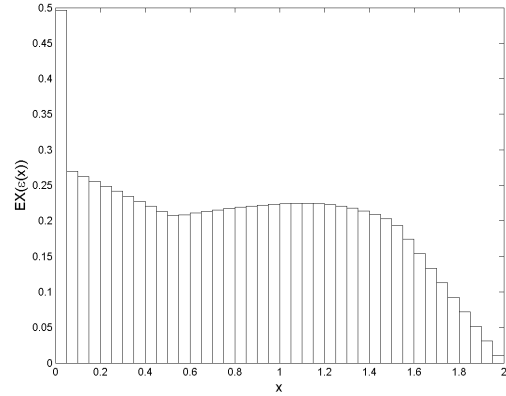
7.1 FEM examples

7.1.1 Structure with non-uniform intensity

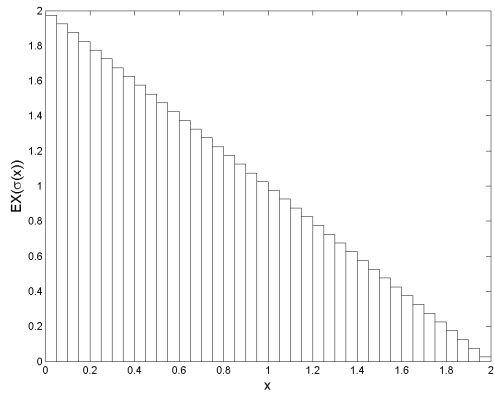
7.1.1.1 Expected values -- Load case a



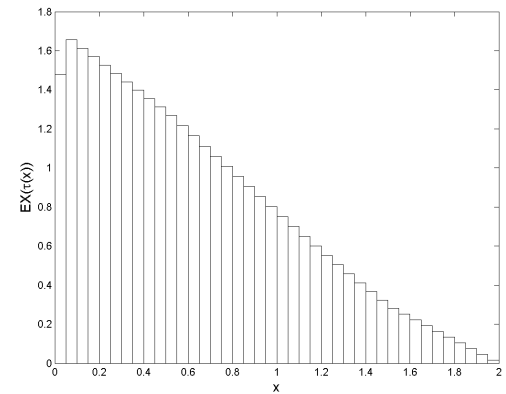
(a) Expected value of displacement $u(x)$



(b) Expected value of strain $\varepsilon(x)$



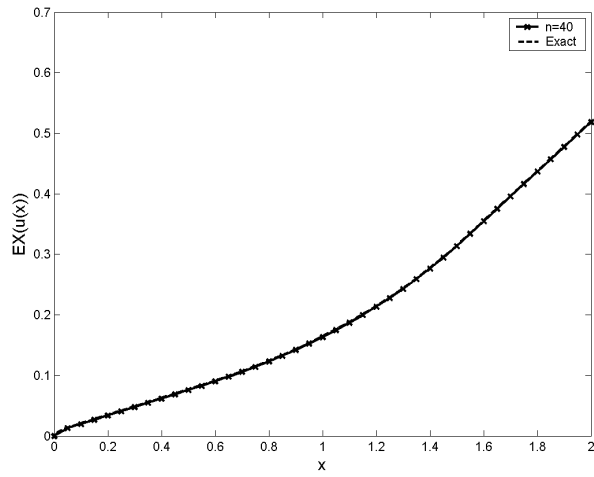
(c) Expected value of stress $\sigma(x)$



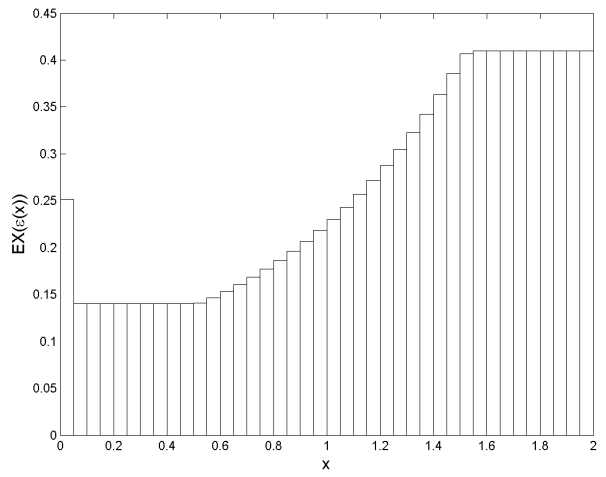
(d) Expected value of stress $\tau(x)$

Figure 13 Expected values, $E_m=2\text{Pa}$, $E_h=20\text{ Pa}$, $L=2\text{m}$, $l=0.05\text{m}$

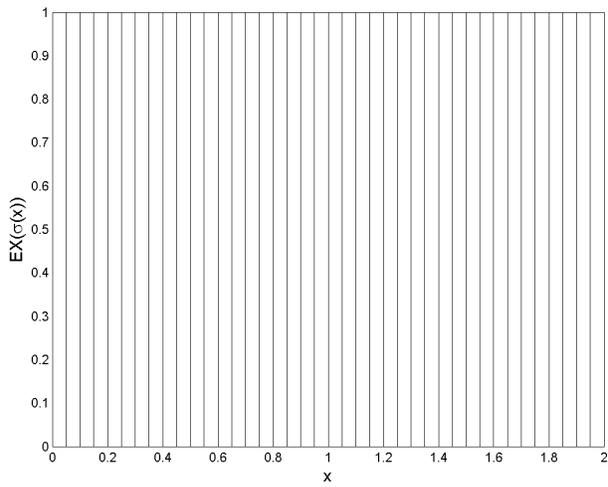
7.1.1.2 Expected values -- Load case b



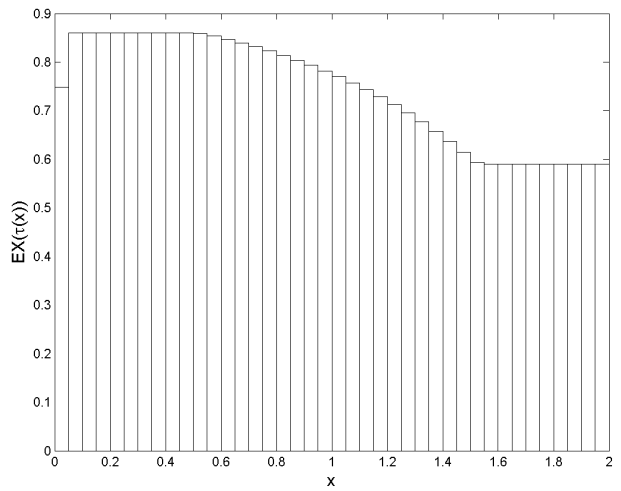
(a) Expected value of displacement $u(x)$



(b) Expected value of strain $\varepsilon(x)$



(c) Expected value of stress $\sigma(x)$



(d) Expected value of stress $\tau(x)$

Figure 14 Expected values, $E_m=2\text{Pa}$, $E_h=20\text{ Pa}$, $L=2\text{m}$, $l=0.05\text{m}$

7.1.1.3 Convergence study--Influence of ratio of E_m/E_h

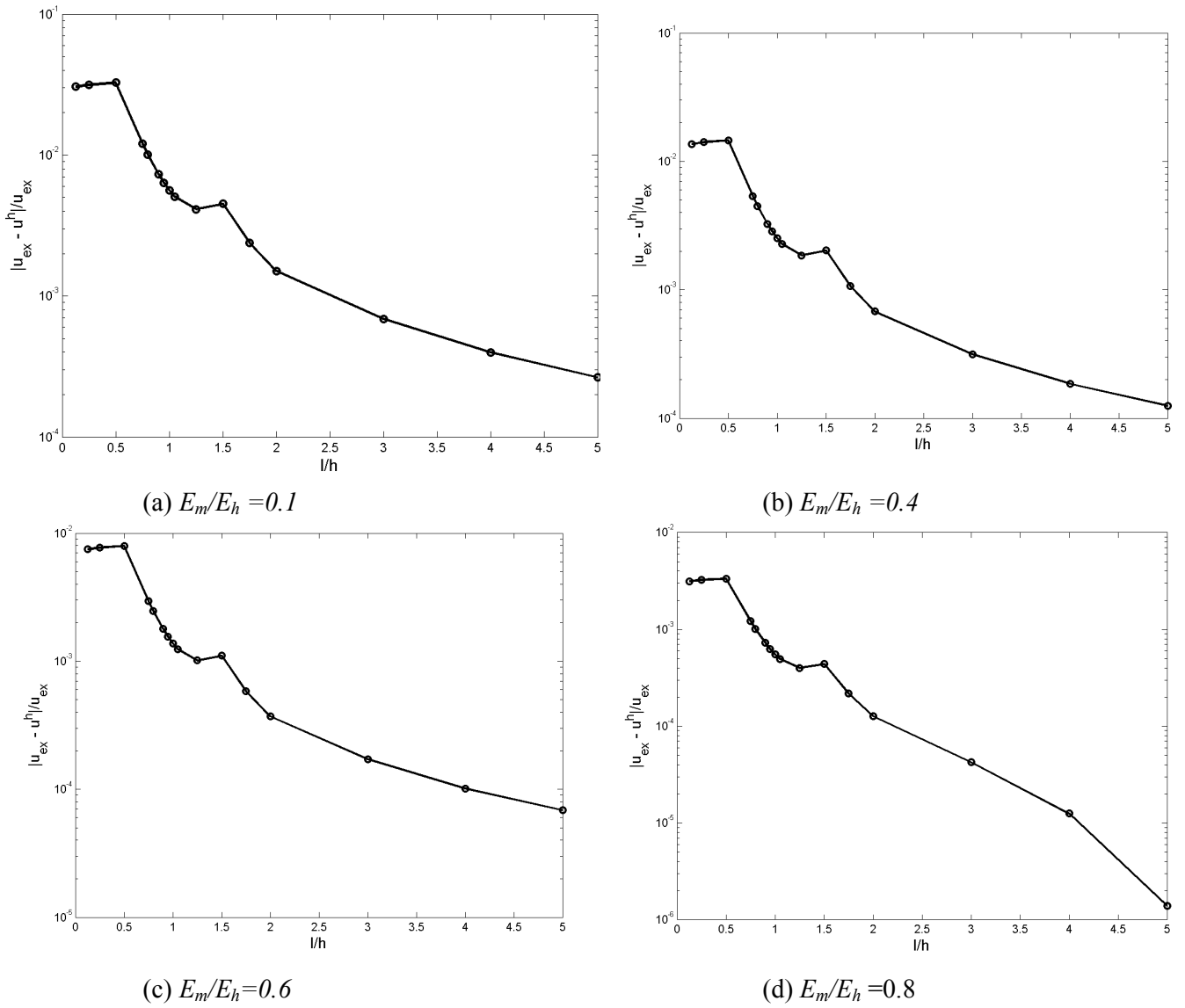


Figure 15 Influence of E_m/E_h on convergence of FEM

7.1.1.4 Convergence study -- Influence of size of the microstructure l

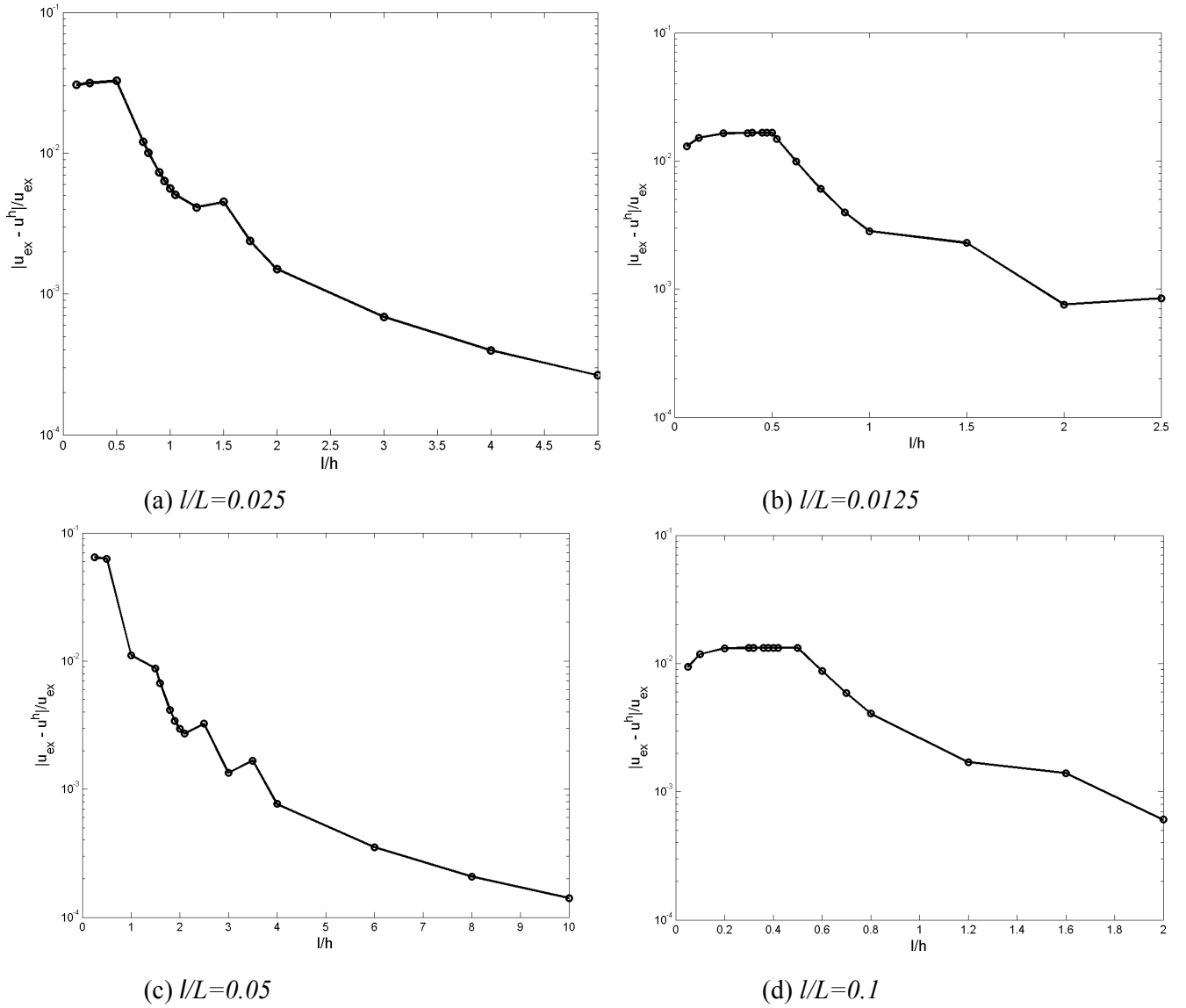


Figure 16 Influence of l/L on convergence of FEM

7.1.2 Example of structure with uniform intensity

Expected values -- Load case a

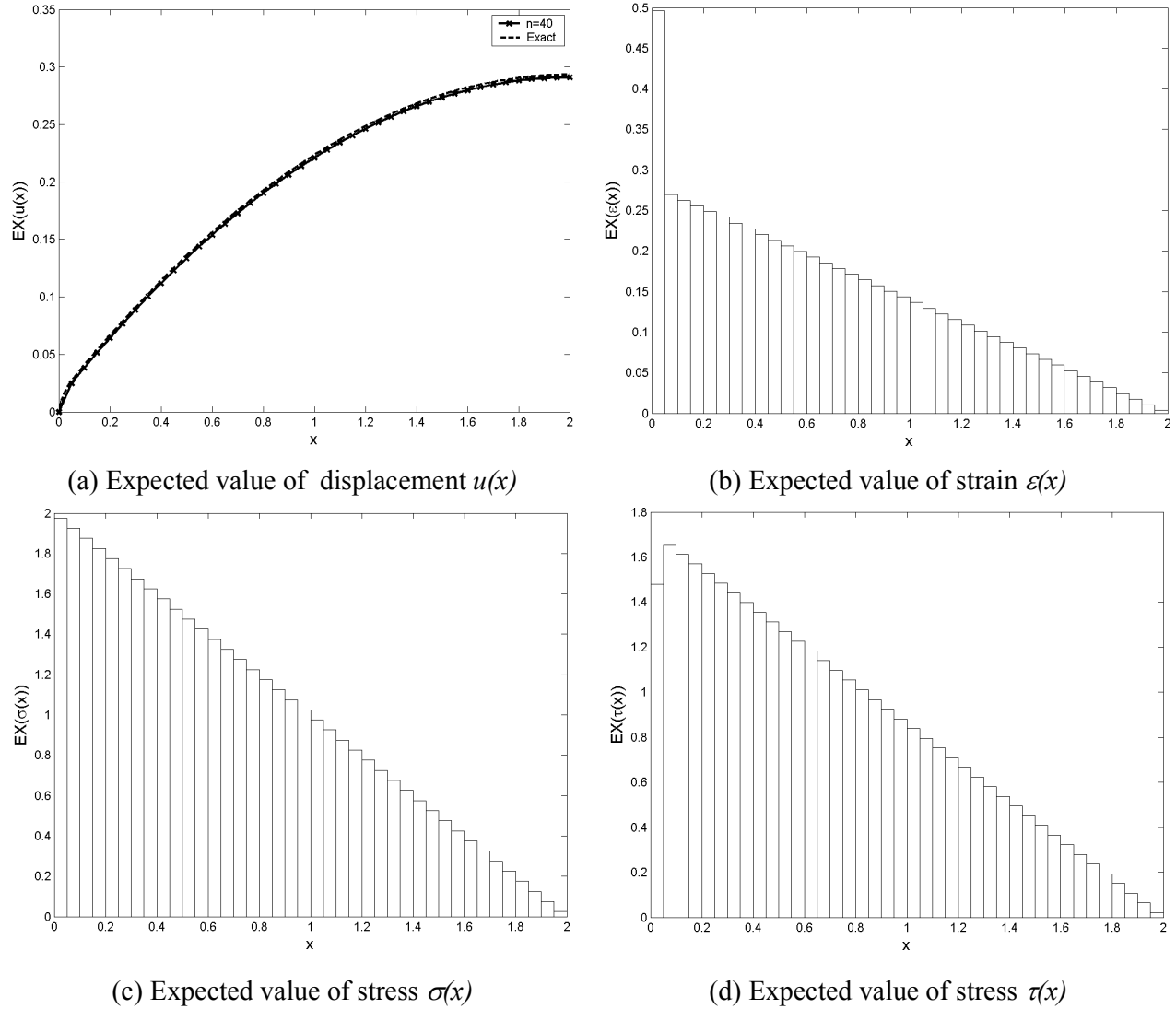


Figure 17 Expected values, $E_m=2\text{Pa}$, $E_h=20\text{ Pa}$, $L=2\text{m}$, $l=0.05\text{m}$

7.2 BEM examples

7.2.1.1 Expected value - Load case a:

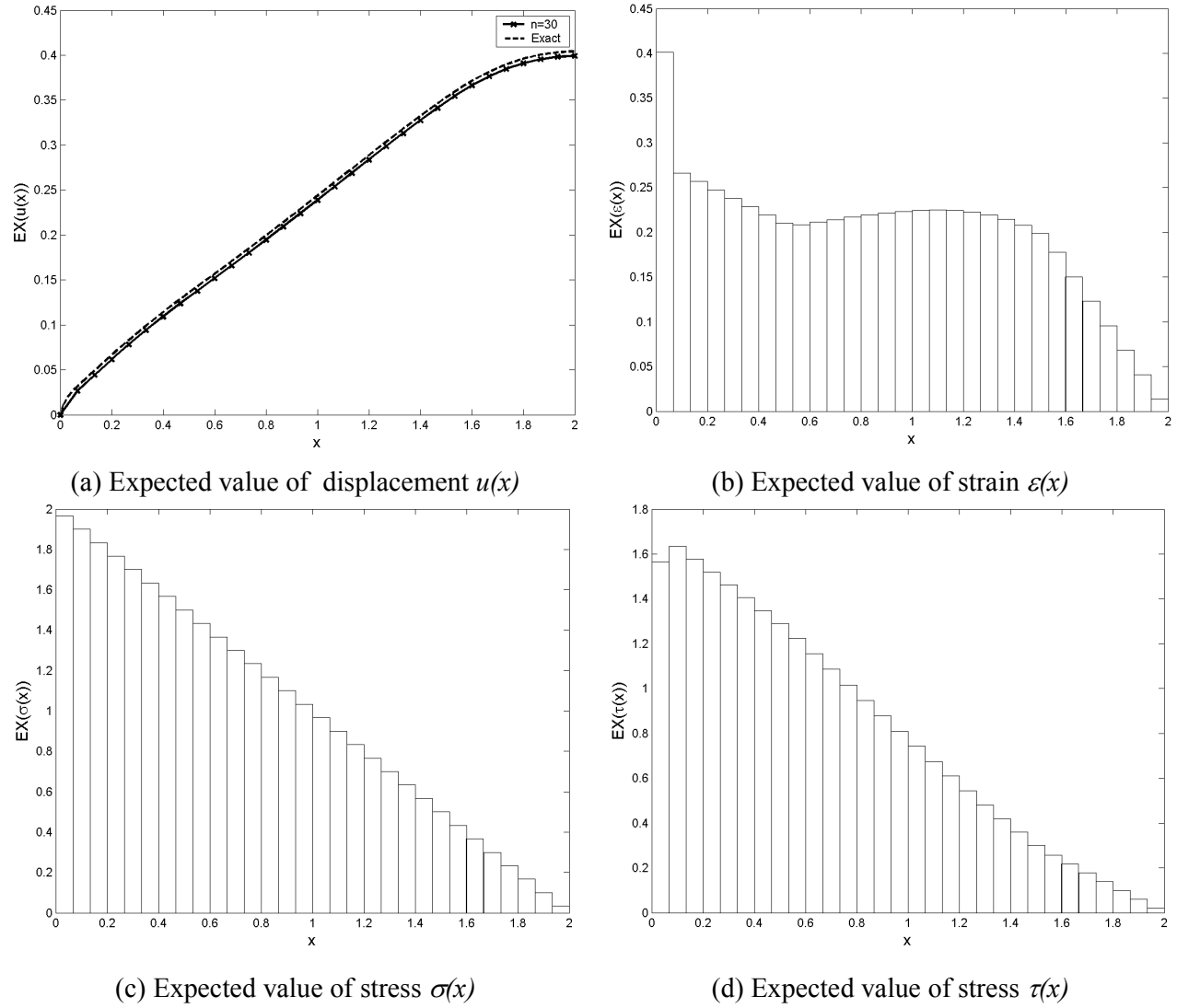
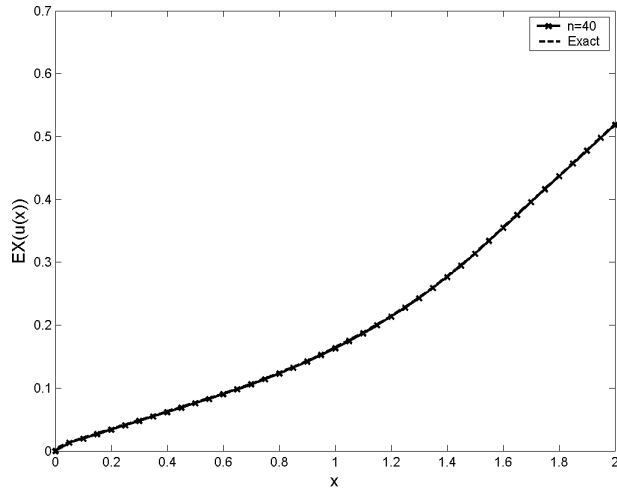


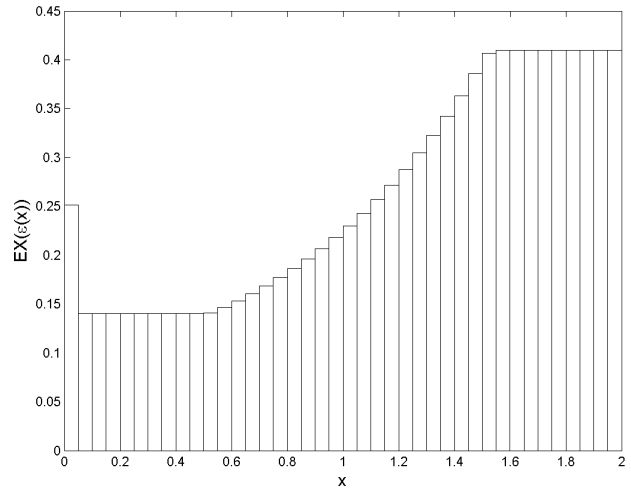
Figure 18

Expected values, $E_m = 2\text{Pa}$, $E_n = 20\text{Pa}$, $L = 2\text{m}$, $l = 0.05\text{m}$

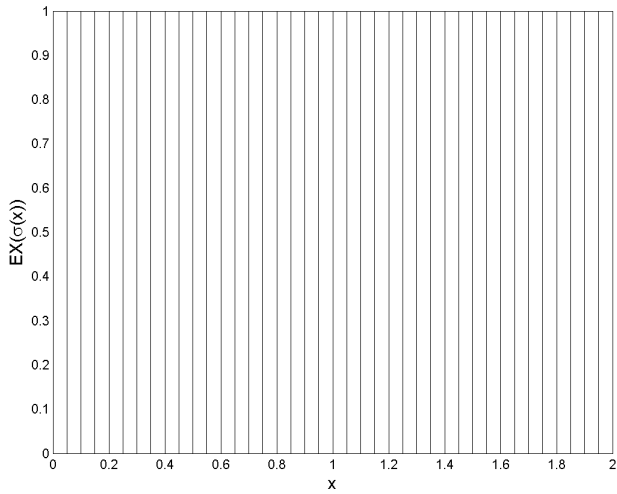
7.2.1.2 Expected value - Load case b:



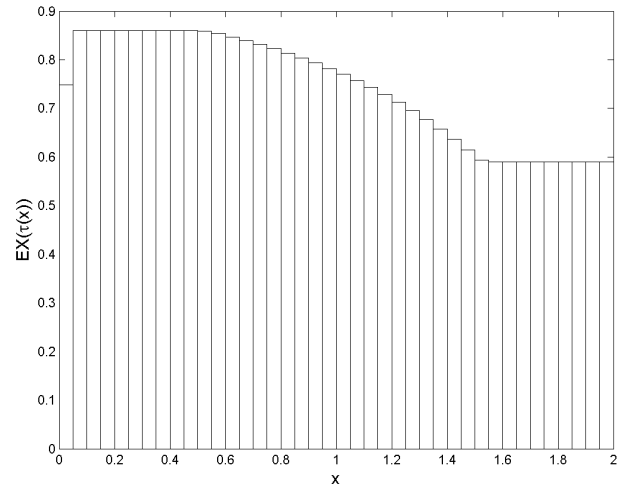
(a) Expected value of displacement $u(x)$



(b) Expected value of strain $\varepsilon(x)$



(c) Expected value of stress $\sigma(x)$



(d) Expected value of stress $\tau(x)$

Figure 19 Expected values, $E_m = 2\text{Pa}$, $E_n = 20\text{ Pa}$, $L = 2\text{m}$, $l = 0.05\text{m}$

8 Conclusions and future work

From the results of the graphs, it can be concluded that FEM and BEM Hashin-Shtrikman approximations give identical results, which can be seen from the graph convergence of both methods

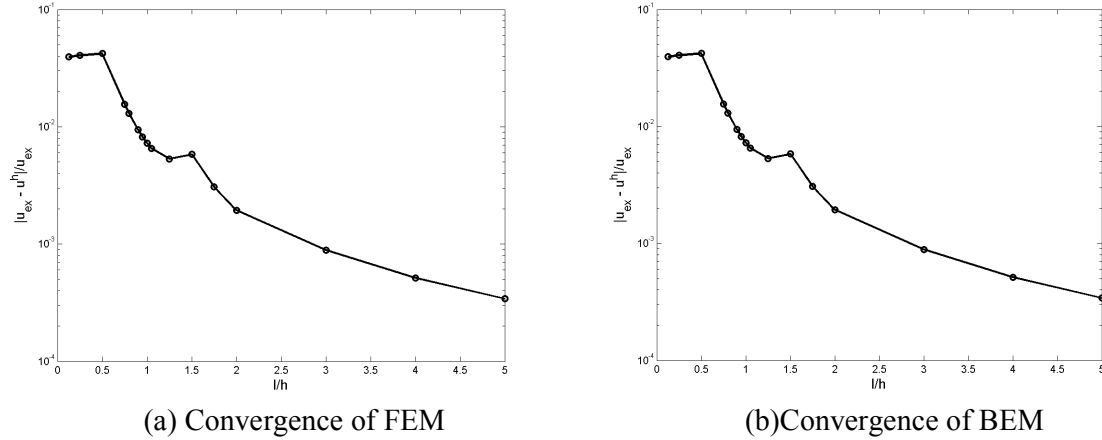


Figure 20 Comparison FEM/BEM

The factors that influence the convergence are the size of microstructure, l/L , and the ratio of E_m/E_h . It can be seen from the Figure 12 and Figure 13 that the closer is the ratio of E_m/E_h to one and the bigger l/L are, the more accurate the solution is.

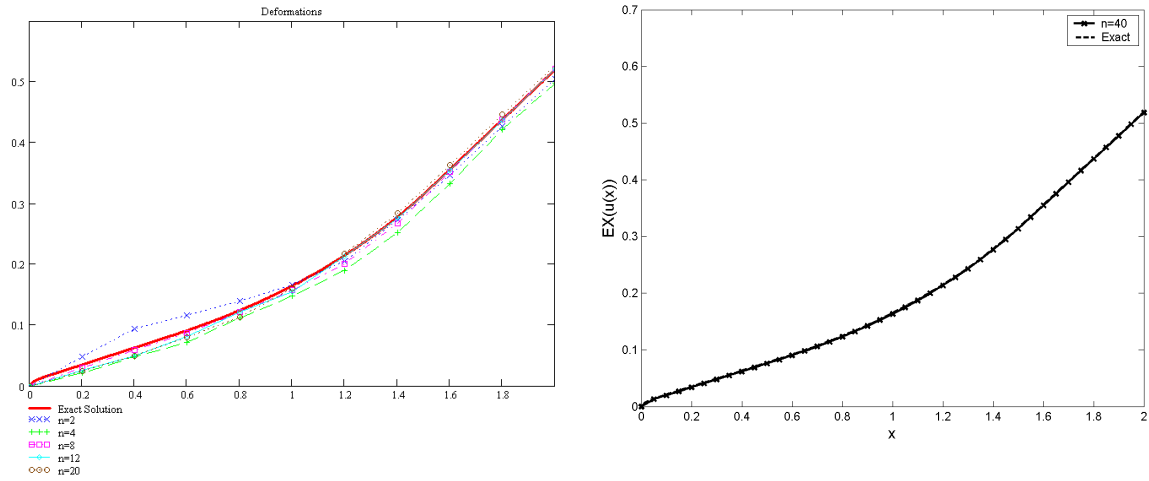
Comparing the both methods, homogenization method and variation by Hashin-Shtrikman method, it can be concluded that the Hashin-Shtrikman variation gives good enough result and is more convenient to use since it takes much less time for calculation compared to homogenization method. Both results can be seen in the figure below:

In general, the difference between two numerical methods can be summarized as follows

- Solution of the homogeneous problem
 - **FEM:** The structure is divided into n finite elements and for each element the displacement u is computed. Solution on $n \times n$ sparse system of equations is needed.
 - **BEM:** The structure is divided into infinite bodies and the equations contain only boundary integrals. It relates the value of u at some point inside the domain to an integral expression involving u and $\frac{\partial u}{\partial n}$ over the boundary. The dimension of the linear system to be solved is by one order less than for FEM.
- Solution of the stochastic problem
 - **FEM:** For stochastic solution, the Green's function is needed which in the case of FEM, the discrete Green's function is evaluated. This is quite a costly part of the algorithm.
 - **BEM:** In this case, the Green's function is assumed to be known, only Γ_r needs to

be evaluates which is a constant value added to Green's function for the infinite body. This presents a significant advantage when compared to the FEM.

For both methods, a symmetric dense $n \times n$ system of equations is solved. In this step, BEM formulation does not have any advantage over the FEM.



(a) Displacement $u(x)$ from Monte-Carlo simulation

(b) Displacement $u(x)$ from Hashin-Shtrikman variational method

Figure 21 Comparison of results from the statistical and the numerical methods

In the future work, the next logical step is to generalize the solution to more dimensions. This is, however, a rather complicated task which goes beyond the scope of the diploma project. Once this step is completed, the resulting formulation is very well suited for optimization studies of statistically inhomogeneous material systems. The specific non-linear behavior of materials can also be considered. Hopefully, these topics will be covered in the future research work.

9 References

- [1] J. Quintanilla and S. Torquato, Microstructure functions for a model of Statistically Inhomogeneous Random Media, *Physical Review E*, 55, 1558 (1997).
- [2] K. Rektorys, *Survey of Applicable Mathematics, Volumes II*, Springer Verlag, 1999, Second edition
- [3] J.Q.Li, X.R.Zeng, J.N.Tang, P.Xiao Fabrication and thermal properties of a YSZ–NiCr joint with an interlayer of YSZ–NiCr functionally graded material, *Journal of European Ceramic Society*, 23, 1847-1853, 2003
- [4] R. Luciano, J.R. Willis, *Journal of the Mechanics and Physics of solids* 53,1505–1522, 2005
- [5] Z. Bittnar, J. Šejnoha, *Numerical Methods in Structural Mechanics, Numerical Methods in Structural Mechanics*, American Society of Civil Engineers, 1996
- [6] P. Procházka and J. Šejnoha, Extended Hashin-Shtrikman variational principles, *Applications of Mathematics*, 49, 357 – 372, 2004

- [7] P. Brož a P. Procházka, Boundary element method in engineering practice, SNTL, 1987, Praha, (In Czech)
- [8] P. Hunter, A. Pullan, FEM/BEM notes, The university of Auckland, New Zealand, Feb.19, 2002.
- [9] J. Zeman, Analysis of composite materials with random microstructure, CTU Reports, 7, 2003, Czech Technical University in Prague
- [10] Procházka, P. and Šejnoha, J. BEM formulation for homogenization of composites with randomly distributed fibers, Engineering Analysis with Boundary Elements, 27, 137-144, 2003
- [11] Achim Neubrand and Jurgen Rodel, Gradient materials: An overview of a novel concept, Fachbereich material wissenschaft fer TH Darmstadt, Germany

10 Appendices

In the appendices, a substantially shortened version of the codes used to compute the presented results is gathered. In particular, Section 10.1 described code used for Monte-Carlo simulations written in MathCAD®, while Sections 10.2 and 10.3 show excerpts from the Hashin-Shtrikman algorithm in MATLAB® environment.

10.1 Simulation method

10.1.1 Non-uniform intensity

l is the fiber length, L is the rod length

$$L := 2$$

$$\rho_a := \frac{-\ln(0.2)}{l} \quad \rho_b := \frac{-\ln(0.8)}{l}$$

Intensity function:

$$\rho(x) := \begin{cases} \rho_a & \text{if } 0 \leq x < a \\ \rho_a + \left(\frac{\rho_b - \rho_a}{b - a} \right) (x - a) & \text{if } a \leq x < b \\ \rho_b & \text{if } b \leq x \leq L \end{cases}$$

t is a generation of the geometry

$$t := \text{Range}(0, L)$$

$$n_f := \sum_x \begin{cases} \text{for } i \in 0.. \text{length}(t^{(0)}) - 1 \\ x_i \leftarrow \text{if}(t_{i,1} - t_{i,0} = 1, 1, 0) \end{cases} \quad \begin{array}{l} n_f \text{ counts the number of the fibres in the rod} \\ \text{if the length of the segment } t_{i,1} - t_{i,0} \text{ is } d \text{ then a fiber is there} \end{array}$$

$$\text{seq} := \begin{cases} \text{for } k \in 0.. \text{length}(t^{(0)}) - 1 \\ i_k \leftarrow \text{if}(t_{k,1} - t_{k,0} = 1, 1, 0) \\ i \end{cases}$$

seq is the characteristic function:
 If seq=1 $\Rightarrow \chi_m(x)=1 \Leftrightarrow x$ is in the matrix phase
 If seq=0 $\Rightarrow \chi_f(x)=1 \Leftrightarrow x$ is in the fiber phase

f1(x) := 2 f1(x) and f2(x) is the value E1 and E2 for the matrix and
 f2(x) := 20 fibers respectively

$$E(x) := \begin{cases} \text{rng} \leftarrow t^{(1)} \\ n \leftarrow 0 \\ \text{while } x \geq \text{rng}_n \\ n \leftarrow n + 1 \\ k \leftarrow \text{seq}_n \\ f_k \cdot x \end{cases}$$

E(x) assigns the values f1 and f2 to the fibers
 using the range and seq.
 k <- seq_n: For seq=0 use f1, for seq=1 use f2

$$\sigma(x) := \frac{N(x)}{A} \quad \text{Normal stress}$$

$$N(x) := [N + f_x \cdot (L - x)]$$

$$\varepsilon(x) := \frac{\sigma(x)}{E(x)} \quad \text{Normal strain}$$

$$u(x) := \left(\int_0^x \varepsilon(x) dx \right) \quad \text{Deformation}$$

LOOP:

n is the number of times (different rods)

M generates z different samples (geometries) for n realizations:

$$M := \begin{cases} \text{for } t \in 0.. 4 \\ \text{for } i \in 0.. k_t - 1 \\ m_{i,t} \leftarrow \text{Range}(0,L) \\ m \end{cases}$$

$$c_m(x) := \begin{cases} \exp(-\rho_a \cdot x) & \text{if } 0 \leq x \leq 1 \\ \exp(-\rho_a \cdot 1) & \text{if } 1 < x \leq a \\ \exp\left[-\rho_a \cdot 1 - \frac{\rho_b - \rho_a}{2} \frac{b-a}{(x-a)^2}\right] & \text{if } a < x \leq a + 1 \\ \exp\left[-\rho_a \cdot 1 - \frac{\rho_b - \rho_a}{2} \cdot [2 \cdot (x-a) - 1]\right] & \text{if } a + 1 < x \leq b \\ \exp\left[-\rho_b \cdot 1 + \frac{\rho_b - \rho_a}{2} \frac{b-a}{(x-b-1)^2}\right] & \text{if } b < x \leq b + 1 \\ \exp(-\rho_b \cdot 1) & \text{if } b + 1 < x \leq L \end{cases}$$

Local volume fraction matrix:

Expected value of E(x):

$$EX\varepsilon(x) := c_m(x) \cdot f1(0) + (1 - c_m(x)) \cdot f2(0)$$

Theoretical (expectation) value for displacement u (EX(u(x))):

$$EXu1(x) := \frac{1}{A} \left(\int_0^x N(x) \cdot \frac{1}{EX\epsilon(x)} dx \right)$$

$$\sigma(x) := \frac{N(x)}{A} \quad \epsilon(x,t) := \frac{\sigma(x)}{T(x)_t} \quad u(x,t) := \left(\int_0^x \epsilon(x,t) dx \right)$$

$$u(x) := \left| \begin{array}{l} \text{for } t \in 0..4 \\ u_t \leftarrow u(x,t) \\ u \end{array} \right. \quad U := \left| \begin{array}{l} \text{for } t \in 0..4 \\ x \leftarrow 0 \\ \text{for } l \in 0..10 \\ \left| \begin{array}{l} a_{t,l} \leftarrow u(x)_t \\ x \leftarrow x + \frac{L}{10} \end{array} \right. \\ a \end{array} \right. \quad \blacksquare$$

Plot graph U,EXu(x).

10.1.2 Uniform intensity

$l := .05$ $L := 2$ l is the fiber length, L is the rod length

$t := \text{Range}(0,L)$ t is a generation of the geometry

$$n_f := \left| \begin{array}{l} \text{for } i \in 0.. \text{length}(t^{(0)}) - 1 \\ x_i \leftarrow \text{if}(t_{i,1} - t_{i,0} = 1, 1, 0) \\ \sum x \end{array} \right. \quad \begin{array}{l} n_f \text{ counts the number of the fibres in the rod} \\ \text{if the length of the segment } t_{i1}-t_{i0} \text{ is } d \text{ then a fiber is there} \end{array}$$

$$\text{seq} := \left| \begin{array}{l} \text{for } k \in 0.. \text{length}(t^{(0)}) - 1 \\ i_k \leftarrow \text{if}(t_{k,1} - t_{k,0} = 1, 1, 0) \\ i \end{array} \right. \quad \begin{array}{l} \text{seq is the characteristic function:} \\ \text{If seq=1} \Rightarrow \chi_m(x)=1 \Leftrightarrow x \text{ is in the matrix phase} \\ \text{If seq=0} \Rightarrow \chi_f(x)=1 \Leftrightarrow x \text{ is in the fiber phase} \end{array}$$

$f1(x) := 2$ $f1(x)$ and $f2(x)$ is the value $E1$ and $E2$ for the matrix and
 $f2(x) := 20$ fibers respectively

$E(x) := \begin{cases} \text{rng} \leftarrow t^{(1)} \\ n \leftarrow 0 \\ \text{while } x \geq \text{rng}_n \\ \quad n \leftarrow n + 1 \\ \quad k \leftarrow \text{seq}_n \\ \quad f_k x \end{cases}$

$E(x)$ assigns the values f_1 and f_2 to the fibers using the range and seq.
 $k < \text{seq}_n$: For $\text{seq}=0$ use f_1 , for $\text{seq}=1$ use f_2

$\sigma(x) := \frac{N(x)}{A}$ Normal stress
 $N(x) := [N + f_x \cdot (L - x)]$

$\varepsilon(x) := \frac{\sigma(x)}{E(x)}$ Normal strain

$u(x) := \left(\int_0^x \varepsilon(x) dx \right)$ Deformation

LOOP:

n is the number of times (different rods)

M generates z different samples (geometries) for n realizations:

$M := \begin{cases} \text{for } t \in 0..4 \\ \quad \text{for } i \in 0..k_t - 1 \\ \quad \quad m_{i,t} \leftarrow \text{Range}(0, L) \\ \quad m \end{cases}$

p is the array that gathers the ranges and the intensities

$p := \begin{cases} \text{for } t \in 0..4 \\ \quad \text{for } j \in 0..k_t - 1 \\ \quad \quad y_{j,0} \leftarrow M_{j,t} \\ \quad \quad \quad \frac{m_{j,t}}{L} \\ \quad \quad y_{j,1} \leftarrow \frac{m_{j,t}}{L} \\ \quad \quad y_{j,2} \leftarrow \exp\left(-\frac{m_{j,t}}{L} \cdot l\right) \\ \quad \quad y_{j,3} \leftarrow 1 - \exp\left(-\frac{m_{j,t}}{L} \cdot l\right) \\ \quad \quad y_{j,4} \leftarrow \exp\left(-\frac{m_{j,t}}{L} \cdot l\right) \cdot f_1(0) + \left(1 - \exp\left(-\frac{m_{j,t}}{L} \cdot l\right)\right) \cdot f_2(0) \\ \quad \quad x_t \leftarrow y \\ \quad x \end{cases}$

$$\begin{array}{l}
q := \left| \begin{array}{l} \text{for } t \in 0..4 \\ \left| \begin{array}{l} \text{for } j \in 0..k_t - 1 \\ \left| \begin{array}{l} y_{j,0} \leftarrow \frac{m_{j,t}}{L} \\ y_{j,1} \leftarrow \exp\left(-\frac{m_{j,t}}{L} \cdot l\right) \cdot \frac{1}{f1(0)} + \left(1 - \exp\left(-\frac{m_{j,t}}{L} \cdot l\right)\right) \cdot \frac{1}{f2(0)} \\ x_t \leftarrow y \end{array} \right. \\ \left. \right. \\ \left. \right. \\ x \end{array} \right. \\
EXu(x) := \frac{1}{A} \left(\int_0^x N(x) \cdot EXe_t \, dx \right) \quad EXU := \left| \begin{array}{l} \text{for } l \in 0..10 \\ \left| \begin{array}{l} e_l \leftarrow EXu\left(\frac{l \cdot L}{10}\right) \\ e \end{array} \right. \\ \left. \right. \\ \left. \right. \\ e \end{array} \right. \\
\sigma(x) := \frac{N(x)}{A} \quad \varepsilon(x,t) := \frac{\sigma(x)}{T(x)_t} \quad u(x,t) := \left(\int_0^x \varepsilon(x,t) \, dx \right) \\
r(x) := \left| \begin{array}{l} \text{for } t \in 0..4 \\ \left| \begin{array}{l} \text{for } j \in 0..k_t - 1 \\ \left| \begin{array}{l} v_{t,j} \leftarrow \int_0^x \frac{\sigma(x)}{E(x,j,t)_{j,t}} \, dx \\ \left. \right. \\ \left. \right. \\ v \end{array} \right. \\ \left. \right. \\ \left. \right. \\ v \end{array} \right. \\
u(x) := \left| \begin{array}{l} \text{for } t \in 0..4 \\ \left| \begin{array}{l} u_t \leftarrow u(x,t) \\ \left. \right. \\ \left. \right. \\ u \end{array} \right. \\ \left. \right. \\ \left. \right. \\ u \end{array} \right. \\
U := \left| \begin{array}{l} \text{for } t \in 0..4 \\ \left| \begin{array}{l} x \leftarrow 0 \\ \text{for } l \in 0..10 \\ \left| \begin{array}{l} a_{t,1} \leftarrow u(x)_t \\ \left. \right. \\ \left. \right. \\ x \leftarrow x + \frac{L}{10} \\ \left. \right. \\ \left. \right. \\ a \end{array} \right. \\ \left. \right. \\ \left. \right. \\ a \end{array} \right.
\end{array}$$

Plot graphs U, EXu(x).

10.2 Hashin-Shtrikman FEM method

Appendix[b] - FEM_Hashin-Shtrikman method

```
function [x,xi,EXu,EXe,EXs,EXTau ] = fem_hs( rho, n, E, E_0, L, l, F, f )
```

- Step 1 - Initialization

```

h = L / n;   Length of one finite element
x = Location of nodal points
xi= Location of integration points

```

- Step 2 - Solution of homogeneous problem

-computes the FEM approximation to the homogeneous solution of the problem of a 1D rod of length L with left end clamped and right end loaded by force F subject to the uniform loading with intensity. The structure has Young's modulus E_0 and is discretized into n linear finite elements.

-h =Size of the finite element

-Assemble the stiffness matrix K

-Assemble the vector of generalized loading

-Solve the system of equilibrium equations $Kr = R$

-Geometric matrix

-Get Green's functions

- **Step 3 - Geometry analysis**

-c_m = volume fraction

-S_mm = two point probability

-Function to compute local volume fractions at point x model of fully penetrable intervals of length l distributed randomly on interval $\langle 0, L \rangle$. The expected number of intervals is described by function ρ .

- **Step 4 - Hashin-Shtrikman approximation**

-E : (num_materials, 1) matrix of material parameters

-E0 : reference material

-c_m: (n, 1) matrix of local volume fractions at element integration points

-Gamma_h : (n, n) matrix of Green's function at element integration points

-n : number of finite elements

-h = Length of one element

-num_m = Number of materials

-Set stiffness matrix

-Set the diagonal values

-Reshape the matrix

$K = \text{diag}(K);$

-Right hand side vector R

-Solve the system

$\tau = K \setminus R$

-Determine values of τ in individual phases

- **Step 5 - Post-processing of results**

-num_m= Number of phases

-EXTau = Expected value of polarization stresses

```

-Strain postprocessing
-EXe = e_0 - Gamma * EXtau * h;
-Stress postprocessing
EXs = E_0 * EXe + EXtau;
-Displacement postprocessing
EXu = u_0; Reference homogeneous solution

```

Example:

Example of FEM solution

```

Geomety of microstructure
L = 2.; Macroscopic length of the stucture
l = .05; Microscopic dimension of heterogeneity
Mechanical parameters
E = [ 2., 20. ]; Young's moduli of individual phases [ E_m, E_h ]
E_0 = .5 * min( E ); Reference value of Young's modulus
Loading
F = 0.; End force
f = 1.; Intensity of distributed load
Discretization
n = 40; Number of finite elements
Solve problem
Plot solution

```

10.3 Hashin-Shtrikman BEM method

Appendix[c] - BEM_Hashin-Shtrikman method

- Step 1 - Initiation
 - h = L / n; Length of one finite element
 - x = Location of nodal points
 - xi = Location of integration points
- Step 2 - Solution of homogeneous problem
 - Assemble the stiffnes matrix K
 - Assemble the right hand side R
 - Solve the system $r = K \setminus R$;
 - Evaluate u_0 displacements
 - Boundary values
 - $u_0(1) = r(1)$;

- ```

 u_0(n) = r(2);
- Evaluate Gamma_R
- Change RHS
 R = [1, -1, 0., 0.]
- Solve system again
 r_0 = K \ R;

```
- **Step 3 - Geometry analysis**

```

-c_m = volume fraction matrix
-S_mm = two point probability
-volfrac_m(rho, x, l, L) Function to compute local volume
fractions at point x model of fully penetrable intervals of
length l distributed randomly on interval <0,L>. The expected
number of intervals is described by function rho.
-compute two-point probability function Smm(x,x) for a model of
fully penetrable rods of length l on interval <0,L>

```
  - **Step 4 - Hashin-Shtrikman approximation**

```

- E : (num_materials, 1) matrix of material parameters
- E_0 : reference material
- c_m : (n, 1) matrix of local volume fractions at element
integration points
- Gamma_h : (n, n) matrix of Green's function at element
integration points
- n = Number of elements
- h = L / n; Length of one element
- num_m = Number of materials
- Set stiffness matrix
- S_mm based part of the stiffness matrix
- Assemble stiffness matrix
- Right hand side vector R
- Solve the system tau = K \ R
- Determine values of tau in individual phases

```
  - **Step 5 - Post-processing of results**

```

- num_m = Number of phases
- h = y(2) - y(1); Step of discretization
- Expected value of polarization stresses
- Strain postprocessing
- Stress postprocessing
EXs = E_0 * EXe + EXtau
- Displacement postprocessing

```

$$EXu = EXu + u_0$$

**Example:****Example of BEM solution**

Geometry of microstructure

L = 2.; Macroscopic length of the structure

l = 0.05; Microscopic dimension of heterogeneity

intensity\_function = Gradation profile

Mechanical parameters

E = [ 2., 20. ]; Young's moduli of individual phases [ E\_m, E\_h ]

E\_0 = .5 \* min( E ); Reference value of Young's modulus

Loading

F = 1.; End force

f = 0.; Intensity of distributed load

Discretization

n = 40; Number of finite elements

Solve problem

Plot solution

BEM-Convergence:

Function to plot convergence of function u -> u\_exact